Article:
Yang, D., Huang, S.-S. orcid.org/0000-0003-2816-7104, Liu, F. et al. (1 more author) (2022) Structural fire design of square tubed-reinforced-concrete columns with connection to RC beams in composite frames. Journal of Building Engineering, 57. 104900.

https://doi.org/10.1016/j.jobe.2022.104900

Dongdong Yang, Shan-Shan Huang, Faqi Liu*, Hua Yang. Structural fire design of square tubed-reinforced-concrete columns with connection to RC beams in composite frames, Journal of Building Engineering, July 2022, DOI: 10.1016/j.jobe.2022.104900

Structural fire design of square tubed-reinforced-concrete columns with connection to RC beams in composite frames

Dongdong Yang [a], Shan-Shan Huang [b], Faqi Liu [c,d,*], Hua Yang [c,d]

[a] *Department of Civil Engineering, College of Architectural Science and Engineering, Yangzhou University, Yangzhou, 225127, China*

[b] *Department of Civil and Structural Engineering, The University of Sheffield, Sir Frederick Mappin Building, Mappin Street, Sheffield S1 3JD, UK*

[c] *Key Lab of Structures Dynamic Behaviour and Control (Harbin Institute of Technology), Ministry of Education, Heilongjiang, Harbin 150090, China*

[d] *Key Lab of Smart Prevention and Mitigation of Civil Engineering Disasters (Harbin Institute of Technology), Ministry of Industry and Information Technology, Heilongjiang, Harbin 150090, China*

Abstract

The tubed-reinforced-concrete (TRC) column is an innovative type of steel-concrete composite column that is gaining increasing engineering usage, and structural fire performance should be an important consideration of its design. As affected by the adjacent members and beam-to-column joints, the fire behaviour of TRC columns integrated into a frame may largely differ from that of isolated columns with idealised end conditions. However, the fire performance of TRC columns in composite frames has not been studied, except for some work done on the fire performance of isolated TRC columns with certain

end restraints. This paper presents finite element analysis on single-storey and single-span non-sway frames with square TRC columns, employing the software package ABAQUS. The thermal and deformation behaviour, development of axial stress, axial force and bending moment during heating, working mechanism and failure mode of the frame exposed to fire are numerically investigated. The difference between the fire performance of TRC columns in a frame and those of equivalent isolated columns is quantified. The fire resistance of the framed column is found to lie between those of the columns with rotational end restraints and columns with idealised pinned ends. The complex effects of the connected RC beam on the fire behaviour of TRC columns, e.g. the beneficial restraining effect and the negative effect due to restrained differential thermal expansion, are clarified. Finally, a practical fire resistance design approach is proposed for TRC columns considering the continuity and interactions between structural elements within a composite frame.

Keywords: Square Tubed-Reinforced-Concrete Columns; Composite Frames; Fire Resistance; FEA Modelling; Structural Fire Design.

* Corresponding author, F. Liu. E-mail address: fqliu@hit.edu.cn

1. Introduction

As an innovative type of steel-concrete composite columns, the tubed-reinforced-concrete (TRC) columns, also known as steel tube confined reinforced concrete (STCRC) columns, are gaining popularity in high-rise or large-span structures [1, 2]. Fig. 1 shows two examples where TRC columns are used in high-rise buildings, i.e. Qingdao Haitian Centre (245 m in height) and China Resources Xiaojing Bay Hotel (44.6 m in height) [2, 3]. Unlike traditional concrete-filled steel tubular (CFST) columns, the steel tube of a TRC column discontinues at the column-beam connection, as presented in Fig. 1. The axial load applied onto the TRC column is mainly sustained by the inner reinforced concrete (RC) section. The outer steel tube of a TRC column is designed to only provide transverse confinement to the concrete core, to prevent or delay the tube local buckling and to achieve a more effective confinement effect. Over the past few decades, the static and seismic performance of TRC columns at

ambient temperature has been extensively studied by researchers around the world [4-10]. Most of these works have been focused on isolated columns, whereas Li et al. have investigated the hysteretic behaviour of circular TRC columns to steel beams [11] and RC beams [12] frames. TRC columns are found to possess high load-bearing capacity, good ductility, excellent seismic performance and ease of connection to RC beams. Practical design methods of TRC columns are currently available in the Chinese standard JGJ/T471 [13]. In general, the load-bearing capacity and deformation ability of circular TRC columns at ambient temperatures are better than those of the equivalent square counterparts [1, 9, 10, 13], mainly because the steel tube in the former section could provide a more effective and uniform confinement effect to the concrete core than that in the latter.

Structural fire safety design is essential for column members, as their failure may cause a progressive collapse of the whole structure. However, compared to the extensive research on the fire behaviour of steel, CFST and RC columns, the research on the fire performance of TRC columns is still relatively limited. When exposed to fire, TRC columns behave very differently compared to RC columns and CFST columns [2]. Compared to RC columns, the steel tube of TRC columns can effectively prevent the concrete cover from peeling off due to fire spalling and so help maintain the integrity of the concrete section and protect the rebars against heating. The steel tube of a CFST column sustains the axial load directly and expands more than the concrete in fire, thus the axial deformation of the column is highly affected by the axial behaviour of the steel tube, and the tube is prone to local buckling as its axial stress may increase significantly due to differential thermal expansion. Whereas the axial expansion or contraction of a TRC column in fire mainly depends on the inner RC section since the steel tube is mainly subject to tension in the transverse direction. Therefore, in fire conditions, the axial deformation behaviour, axial load distribution within the composite section, the restraints from surrounding structures onto the heated column and the detrimental effect of tube local buckling on the column performance are very different for TRC and CFST columns. The authors have conducted a series of experimental and numerical investigations on the fire and post-fire behaviour of TRC columns [2, 14-21]. In particular, ISO 834 standard fire tests on four circular, five square and two rectangular TRC specimens have been carried out [2,

14, 15] and these experiments are mainly aimed at isolated TRC columns with pinned-pinned boundary conditions. Finite element analysis (FEA) modelling has been sequentially conducted and practical fire resistance design methods for individual pin-ended TRC columns have been developed [14-16]. Contrary to the performance comparison at room temperature, the fire resistance of a circular TRC column is generally lower than that of an equivalent square one [22]. This is mainly because, compared to the square columns, the axial compressive resistance of circular TRC columns relies more on the confinement effect provided by the steel tube, whereas this confinement decreases quickly in fire due to the fast temperature rising and severe material degradation of the steel tube.

Different from the pin-ended TRC columns, the fire performance of the columns in a frame is highly affected by the structural continuity of the frame and the interactions with adjacent structures (columns, beams and beam to column connections). So far, the fire behaviour of TRC columns in a frame has never been investigated and relevant practical structural fire design methods are lacking. As an initial effort to study the fire performance of TRC columns in a frame, the authors have numerically investigated the behaviour of end-restrained individual square TRC columns exposed to fire [23]. The effects of surrounding structures were simplified as axial and rotational restraints at column ends. Practical design methods were then proposed to account for the effects of end restraints on the fire resistance of TRC columns. However, this approach, i.e. simplifying a column in a frame into an isolated column with end restraints, could not fully consider the complex interactions between structural elements in a composite frame subject to fire. For instance, the simplified approach cannot account for the influences of thermal expansion of and bending moments transferred from heated beams on the deformations and internal forces of TRC columns.

In this work, numerical and analytical investigations are conducted on composite frames with TRC columns subject to fire. Although the confinement effect generated in square TRC columns is generally worse than that in the circular ones, the former columns also possess excellent structural performance as well as good construction and building advantages, and have gained wide applications in engineering [1-3]. Due to the scope of the project, this paper mainly focuses on the fire performance analysis and design of frames formed of square TRC

columns, on the basis of the previous studies conducted on pin-ended and end-restrained square TRC columns [2, 15, 16, 23]. This study aims to: (1) build a 3D FEA model that is capable of predicting the thermal response and mechanical behaviour of TRC frames exposed to fire, with considering the material and geometric nonlinearities and the effect of the composite action between steel and concrete; (2) investigate the fire behaviour of TRC frames, e.g. temperature distribution, deformation, working mechanism and failure mode and analyse the effects of key parameters on the fire performance of the frame; (3) develop a practical method of the fire resistance design for square TRC columns considering frame behaviour and structural continuity.

2. Model setup and validation

2.1 Setup of the FEA modelling

As far as the authors know, in engineering practices, most of the TRC columns are connected with RC beams rather than steel beams to form composite frames [1-3], since this type of column could be more easily constructed with RC beams. Therefore, this study mainly focuses on the fire performance of square TRC columns in TRC column-RC beam frames. The non-sway frame is a common frame form that widely exists in engineering practices. For instance, the frame in a frame-bracing system could be approximately considered as non-sway, since the sway resistance supplied by the bracing is sufficiently stiff and all horizontal loads are assumed to be resisted by the bracing. Following the fire performance studies conducted by the authors on "non-sway" pin-ended and end-restrained TRC columns [2, 15, 16, 23], non-sway TRC frames are mainly investigated in this study. As an early attempt to study the fire performance of TRC frames, simplified frames, i.e. single-storey and single-span, are modelled. Each model consists of two square TRC columns and one RC beam, as shown in Fig. 2. This research is expected to serve as the basis of future research on multi-storey and multi-span frames. In the FEA modelling, the bottom of the framed TRC column is assumed to be fixed, given that the foundation of a frame structure in engineering is generally constructed to be rigid enough [1-3]. The RC beam is of a T shape to consider the

effect of the RC slab on top, which contributes to the thermal and mechanical behaviour of the frame. The determination of the effective flange width of a T-shaped RC beam is crucial for the analysis of a planar frame. It depends on the web and flange dimensions, the type of loading, the span, the support conditions and the transverse reinforcement, as suggested by EC2 [24]. In this study, the effective width of the beam flange is determined based on the Chinese code GB 50010 [25], which is related to the effective span, width, net spacing and flange height of the beam.

To ensure that the steel tube of the TRC column does not sustain the axial load directly, the steel tube is discontinued at the border between the joint and non-joint zones (i.e. the gap 6 in Fig. 3(a)). Semi-continuous joints with tubes partially through the joint region recommended by the Chinese standard JGJ/T471 [13] are adopted for the RC beam to TRC column connections. As shown in Fig. 3(b), at the semi-continuous joint, rectangular holes are cut in the steel tube to allow the reinforcement bars to run through the joint. The steel tube in the joint zone is thicker than that in the non-joint zone, to minimise the risk of joint failure. More details of this type of joint could be found in JGJ/T471 [13].

Only one-quarter of the composite frame is modelled, utilising the symmetries of geometry and loading, as shown in Fig. 4. The sequentially-coupled thermo-mechanical analysis procedure in ABAQUS is adopted to conduct the FEA modelling on the fire behaviour of square TRC columns in composite frames, including a pure heat transfer model and a fire resistance model. The implicit standard solver, i.e. an incremental iterative solution technique based on the Newton-Raphson method is used to execute the simulation in the mechanical analysis. The meshing of the model for the fire resistance analysis is identical to that for the thermal analysis, to ensure the temperature results calculated via the heat transfer could be properly input into the mechanical model. The element types are DC3D8, DS4 and DC1D2 for concrete, steel and reinforcements, in the heat transfer analysis, respectively. As for the mechanical model, element types C3D8R, S4R and T3D2 are used to model concrete, steel tube and rebar, respectively. It needs to be pointed out that the S4R element, i.e. 4-node quadrilateral stress-displacement shell element with reduced integration and a large-strain formulation, is capable of capturing the possible local buckling of the steel tube in TRC

columns [2, 9, 10, 14-21]. Mesh sensitivity analyses have been conducted on both the thermal and mechanical models to determine the optimum mesh size.

The ISO 834 [26] standard fire is used as the heating curve in the thermal analysis. The bottom surface of the slab and all exposed surfaces of the beam and columns in the lower storey are subject to heating (radiation and convection) directly. A convective coefficient of 25 W/(m^2·K) and an emissivity coefficient of 0.7 are adopted for the heated surfaces. A convective coefficient of 9 W/(m^2·K) is applied to the surfaces that are not exposed to external heating, i.e. the top surface of the slab and the upper storey, to simulate the heat transfer between these parts and the environment [27]. A thermal resistance of 0.01 (m^2·K)/W is considered at the steel tube-concrete interface, as recommended by Ding and Wang [28] and Lv et al. [29]. In the mechanical model, the bottom end of the TRC column is fixed both transitionally and rotationally; its top end is only allowed to move vertically and rotate in plane, and thus the frame is verified to be non-sway. A constant concentrated load N_f is applied onto the top end of the column. The top surface of the beam is subject to a UDL (uniformly distributed load) q_b. The column load ratio n is defined as the ratio of the axial force generated in the column, i.e. the resultant force due to N_f and q_b, to the ambient-temperature buckling resistance of the TRC column in isolation, with pinned top end and fixed bottom end. As for the RC beam, the load ratio m is defined as the ratio of the applied bending moment at the mid span of the beam to its moment resistance at ambient temperature. Specifically, for a set of column load ratio n and beam load ratio m combinations, the UDL q_b input into ABAQUS is first determined according to the reference value of m and the bending resistance of the beam. Then the applied load N_f on the column could be calculated based on the n value and the UDL q_b on the beam.

The thermal property models proposed by Lie [30] are used to determine the specific heat and thermal conductivity of concrete. The influence of water evaporation on heat transfer is considered by modifying the specific heat value of concrete at 100 °C using the method recommended by Han [31], with assuming a moisture content of 5%. The high-temperature mechanical behaviour of concrete is modelled using the compressive stress-strain relationship proposed by Lie [30] and the tensile one developed by Hong and Varma [32]. It

should be noted that the transient creep strain of concrete is implicitly included in the compressive stress-strain model [30]. The tensile strength of concrete at elevated temperatures is taken as 0.09 times of the corresponding compressive strength. As for the steel, the thermal models proposed by Lie [30] are used for the temperature-dependent thermal properties, while the high-temperature constitutive models of structural steel and reinforcement given in EC4 [33] are used for the steel tube and reinforcing bars, respectively. When adopting these material models [33], the effect of high-temperature creep need not be given explicit consideration as it is already included in the total strain.

The reinforcing bars are embedded into the concrete core to achieve deformation compatibility. As for the interface between the steel tube and concrete core, the Coulomb friction formulation with a coefficient of 0.3 and a shear stress limit of 0.4 MPa, is adopted for the tangential behaviour to consider the bond-slip effect. The hard contact is assigned to the normal direction, assuming that only compression could be transferred at the interface. Different shear stress limits are assessed to see whether the bond transfer between steel tube and concrete infill affects the fire behaviour of framed TRC columns. It is found the influence of bond stress on the fire performance of TRC frames is very minor. This is consistent with the conclusion drawn by Ding and Wang [28] on CFST columns. Therefore, a default bond stress of 0.4 MPa, e.g. the limit previously used by the authors for the fire resistance modelling of TRC columns [2, 14-16, 23] and recommended by EC4 [34] for ambient-temperature design and by Tao et al. [35] for post-fire analysis of composite columns, is adopted for all the frames in this study. With using the above simulation approaches in ABAQUS, for example, the surface-to-surface interaction at the tube-concrete interface, the concrete damaged plasticity model, C3D8R element for concrete and S4R element for steel tube, the confinement effect provided by the tube to concrete in TRC columns could be automatically and effectively simulated [2, 9, 10, 14-21]. A load eccentricity of $L/1000$ is applied to the column to consider the initial imperfection of the column, where L is the column length. This initial eccentricity is recommended by Ding and Wang [28] to model the fire behaviour of CFST columns and adopted by Han et al. [36] in the simulation of CFST frames in fire.

To the authors' best knowledge, there is currently not a clear and unified criterion within the structural fire design codes worldwide to define the failure of composite frames. In this study, the failure criteria for isolated beams or columns given in ISO 834 [26] are adopted to define the fire resistance of the frame. For beams, their failure is defined as when the flexural deflection reaches $L_b^2/(400h)$ and the deflection rate is larger than $L_b^2/(9000h)$ after the deflection exceeds $L_b/30$, where L_b (in mm) and h (in mm) are the effective span and height of the beam, respectively. As for columns, their fire resistance is defined as the time when the axial deformation exceeds $L/100$ or when the deformation rate reaches $3L/1000$ mm/min, where L (in mm) is the height of the column. The composite frame is considered to fail once either a column or a beam fails according to the above-mentioned criteria. This approach has also been adopted by Han et al. [37, 38] in the experimental and numerical investigations on the fire behaviour of CFST frames.

2.2 Validation of the FEA modelling

The authors have verified the thermal and mechanical FEA models developed in Section 2.1 using extensive fire test results of isolated columns, including 11 TRC columns, 119 CFST columns and 26 RC columns. The detailed validation results could be found in references [2, 15, 16] and are not repeated here. As far as the authors know, no fire tests on composite frames with TRC columns have been reported. Given that the CFST and TRC columns are similar to some extent, the fire tests on six CFST column-RC beam frames (CFRC-1 to CFRC-4 with circular CFST columns and STRC-1 and STRC-2 with square CFST columns) conducted by Han et al. [37] and two CFST column-steel beam frames (Test 4 and Test 8) reported by Ding and Wang [39] are used to validate the FEA model developed in this study.

2.2.1 Validation against Han et al.'s tests

Each of the six frames was comprised of two CFST columns and one rectangular RC beam. Two example frames after the fire tests are shown in Figs. 5(a) and 5(c); their corresponding models are shown in Figs. 5(b) and 5(d). The details of the six frames, e.g. the dimensions of the beams and columns, the diameters of the longitudinal reinforcing bars, the applied loads

and load ratios onto the beams and columns, and the measured strengths of the steel tube, concrete and rebars, are listed in Table 1. All the CFST columns in these frames were protected with sprayed fire protection material, whose thicknesses were also included in Table 1. To model the fire protection coating in FEA, the DC3D8 element of ABAQUS was used and its inner surface was tied to the outer surface of the steel tube. The thermal properties reported in reference [37], i.e. a thermal conductivity of 0.116 W/(m·K), a specific heat of 1047 J/(kg·K), a density of 400±20 kg/m^3 and a water content of 1%, were adopted. The column was uniformly heated on four sides, while the RC beam was exposed to fire on three sides. As for the RC slab, only the bottom surface was exposed to heating. Other details of these CFST tests, e.g. the boundary conditions, the arrangements of thermocouples and the locations of LVDTs could be found in reference [37].

The FEA predicted failure modes are consistent with those observed in the testing; two examples (CFRC-1 and SFRC-1) are shown in Figs. 5(a)-5(d). Fig. 6 presents the predicted development of temperature over time at different locations of three typical frames (CFRC-2, CFRC-3 and SFRC-1), compared with the test data. Good agreements are generally achieved, except for column temperatures around in the joint zone (Figs. 6(b), 6(f) and 6(j)). Such temperature discrepancies mainly concentrate between 100 °C and 150 °C, mainly because the effects of moisture evaporation and migration are not accurately modelled in FEA. The evolution of the axial deformation at the column top end and that of the flexural deflection of the beam are compared with the test results in Fig. 7. Considering the arrangement of LVDTs, i.e. two identical LVDTs are generally symmetrically located on the columns or beam, only half of the measured displacement is used in the model validation. As presented in Table 1, the average ratio between the numerical fire resistance $t_{R,F}$ and the test result $t_{R,t}$ is 1.06, indicating a good prediction accuracy of the FEA model.

2.2.2 Validation against Ding and Wang's tests

Square CFST columns of dimensions 200 mm × 12.5 mm and circular columns of dimensions 193.7 mm × 10 mm were used for the Frame Tests 4 and 8, respectively. I shape steel beams (178 × 102 × 19UB of S275 steel) were connected to columns with reverse channel

connections. Test 4 is shown as an example in Fig. 8(a); the corresponding model frame is shown in Fig. 8(b). Since these two tests mainly focused on the behaviour of the beam-column connections, only the steel beams were loaded. The top flange of the beam was thermally insulated to simulate the heat sink effect of the concrete slab. The CFST columns and other surfaces of the steel beam were unprotected and exposed to heating directly.

The evolution of the temperature distribution within the test frame was measured during the tests, which was then used in this model validation. More details of these two tests including the material strengths, boundary conditions and applied loads could be found in reference [39]. The failure modes given by the FEA model compare well with the test observations, as exampled in Figs. 8(a) and 8(b). Fig. 9 shows the FEA predicted axial force and mid-span deflection of the steel beams of the Frame Tests 4 and 8, compared with the experimental results [39].

The discrepancies between the FEA predicted mechanical results, e.g. the deformation behaviour, failure mode and fire resistance, and the corresponding test data are mainly attributed to 1) the complexity and result variability of fire tests, especially for frame tests; 2) the assumptions made in the FEA. For example, the temperature-dependent material properties of the specimens have to be assumed in FEA as these are not provided in references [37, 39]. In general, the validation results as illustrated in Figs. 5-9 and Table 1 confirm that the developed FEA modelling is capable of predicting the thermal response, mechanical behaviour, failure mode and fire resistance of CFST frames exposed to fire. This FEA model is, therefore, used in the following sections to analyse the fire behaviour of TRC frames.

3. Modelling results and discussions

Compared to the extensive applications of composite frames with CFST columns in real constructions, the reported usage of TRC composite frames is still relatively limited. Since the mechanical behaviour of both CFST and TRC columns closely relies on the composite actions between the steel tube and concrete core and they could achieve similar load-bearing performance at ambient temperature [2], the TRC frames investigated in this study are designed with reference to an engineering project (Xiamen Jinyuan Building, 1992) using a

CFST column-RC beam frame [36].

The main parameters of the modelled TRC frames are as follows:

1) For the square TRC columns, cross-sectional width B = 600 mm; slenderness ratio λ = 30 and 50; steel ratio α_s = 3%; reinforcement ratio ρ = 4%; yield strength of the steel tube f_y = 345 MPa; The typical load levels of steel-concrete composite columns in the fire limit state are generally between 0.3 and 0.7 [40-42]. For isolated square TRC columns with cross-sectional size no less than 600 mm and slenderness ratio no larger than 30, the fire resistance could generally reach a rate of higher than 180 min when the column load ratio is lower than 0.5. Considering that the end restraints provided by the RC beam could further enhance the column fire resistance, to avoid excessive fire resistance of the framed columns calculated using FEA, the load ratios n applied to column top end are 0.5, 0.6 and 0.7, which is within the common load ratio ranges of composite columns.

2) For the rectangular RC beam, cross-sectional dimensions $H_b \times B_b$ = 650 mm × 400 mm; effective span L_b = 9000 mm; two layers of 2ϕ28 rebars are arranged at the bottom of the beam and one layer of 2ϕ20 is at the top of the beam; load ratio m = 0.3, 0.5 and 0.7.

3) For the RC slab, cross-sectional dimensions $H_s \times B_s$ =120 mm × 3000 mm; effective span L_s = 9000 mm; two layers of ϕ8 rebars are arranged with a spacing of 200 mm.

4) For the column-beam connections, the steel tubes in the non-joint and joint zones are 4.5 mm and 10 mm thick, respectively. The standard JGJ/T471 [13] recommends a 10 mm to 20 mm width for the gap between the steel tubes in the non-joint and joint zones, to ensure that the tubes are not subject to the axial force directly due to their physical contact. Considering the deformations of the column at elevated temperatures are larger than those at ambient temperatures, the upper limit of the gap width, i.e. 20 mm, is used. Trial FEA calculation demonstrates that this width is enough to avoid the direct contact of tubes before the frame reaches fire resistance. The openings in the steel tube in the joint (i.e. 5 in Fig. 3) are designed to JGJ/T471 [13].

5) The yield strength f_b of all the rebars is 335 MPa. The concrete cover c for the rebars is 25 mm. The cylinder compressive strengths of concrete f'_c in the columns, beam and slab are 50 MPa, 40 MPa and 30 MPa, respectively.

It should be noted that the above-described geometries and dimensions of the columns, beams and slabs adopted in this study for TRC frames are the same as those used in the Xiamen Jinyuan Building project. Whereas square TRC columns and semi-continuous joints (as introduced in Section 2.1) are used to replace the square CFST columns and CFST column-RC beam joints in that project, respectively. As for the material properties, e.g. the strengths of concrete, steel tube and rebars, nominal values rather than the real values of that project are adopted in this study.

The thermal response and mechanical performance, e.g. the failure mode, developments of deformations, internal forces and axial stresses, of the TRC columns and RC beams will be discussed in this section, to clarify the behaviour and working mechanism of single-storey and single-span TRC frames in fire.

3.1 Thermal response

The thermal response of the composite frame to heating is analysed. Fig. 10 presents the temperature distributions of the beam, columns and slab at 120 min as an example. As shown in Figs. 10(a) and 10(b), the concrete in the joint is of a lower temperature than the concrete at an equivalent location but out of the joint zone, which is mainly because of the shielding effect of the connected elements onto the joint. The temperature difference between the joint and non-joint zones decreases as heating carries on. During the whole heating period, the temperatures of the unexposed surfaces of the frame remain at relatively low levels, e.g. no higher than 100 °C even after 6 h of heating. Owing to the thermal insulation provided by the concrete cover, the temperatures of the rebars are much lower than those of the steel tubes and thus the former could retain higher strengths and stiffnesses than the latter.

The evolution over time of temperatures at different locations in the joint and non-joint sections of the columns or beam is compared in Fig. 11. As shown in Fig. 11(a), Points C1 to C5 are on the symmetric axis of the column section. In particular, C1 and C2 are at the same physical location, whereas, C1 is on the internal surface of the steel tube and C2 is on the concrete core. As for the beam, Points B1 to B5 locate at different heights along the symmetric axis of the section. Consistent with the observations in Fig. 10, the temperature in

the joint is significantly lower than that in the non-joint zone, which is particularly obvious towards the outer part of the column and towards the bottom of the beam (e.g. Points C1 and B1 in Fig. 11). Thermal resistance is assumed at the interface between the concrete and steel tube in the non-joint section of the column, to consider the effect of the gap between the steel tube and concrete core. Therefore, the temperature at Point C1 on the inner surface of the steel tube is higher than that at the corresponding Point C2. As for the joint zone of the column, it is assumed that the temperatures on the steel tube and concrete at their interface are identical, because the steel tube is embedded in concrete in the joint and the interfacial gap could generally be ignored.

3.2 Failure mode

Taking two frames of column load ratio $n = 0.5$, beam load ratio $m = 0.7$ and $n = 0.7$, $m = 0.3$ as examples, Fig. 12 shows the development over time of the axial deformation of the TRC column top and the flexural deflection at the RC beam mid span. Positive deformations in this figure correspond to the axial elongation of the columns and upward deflection of the beam. It should be noted that the deflection of the beam shown in this figure is the net deflection, which is the deflection at the beam mid span subtracting the deflection at the beam end. As heating proceeds, the overall deformations of the beam and columns increase gradually. The TRC columns in the frame experience no axial elongation and the axial contraction at the column top generally consists of two phases, i.e. an almost linear ascending phase, followed by the runaway phase. This is consistent with the observations from isolated TRC columns under pin-ended boundary conditions and with end restraints [2, 15, 16, 23]. As the load ratios increase, both the axial deformation of the column and the deflection of the beam increase significantly. The failure of both frames is defined as when the axial deformation rate of the columns reaches the limit given in ISO 834 [26], as mentioned above in Section 2.1, i.e. $3L/1000$ mm/min, and their fire resistances are marked with the red dots in Fig. 12.

As the load levels of composite columns in fire conditions are generally around 0.5 [42], the frame with the column load ratio of 0.5 is used as an example to show the typical failure

mode. Fig. 13 illustrates the deformation shape and failure mechanism of the composite frame (n = 0.5, m = 0.5). The column section of the largest lateral deformation occurs close to the top of the column, i.e. approximately 2.1 m from the loaded end of the column. This is mainly due to the unequal boundary conditions at the ends of the column, i.e. the restraint provided by the RC beam at the top end is weaker than the fixed boundary condition at the bottom end. The bending moment due to the second-order effect is also the largest at the section of the largest lateral deformation. As expected, the RC beam experiences the largest flexural deflection at its mid span. It is expected that plastic hinges will form at the sections where the column and beam experience the largest deflections. Therefore, these sections are defined as the control sections of the frame. The internal forces in these control sections during heating are discussed in detail in Section 3.3 to reveal the working mechanism of the frame in fire. The sign conventions of the axial forces and bending moments presented in Fig. 13 are defined as follows: for axial force, tension is positive and compression is negative; for the bending moment of the beam, sagging bending moment is positive and hogging is negative; for the bending moment of the column, it is positive when the column bends outwards, and it is negative when the column bends towards the inside of the frame.

As shown in Fig. 13(b), when the frame reaches the fire resistance limit, the mid span of the beam is under axial tension and positive bending moment; the joint zone of the beam is subjected to axial tension, negative bending moment and upward shear force; the section of the column of the largest lateral deformation is under axial compression, positive bending moment and outward shear force. As the applied load onto the beam remains constant during heating, the development of the negative bending moment at the beam end could generally lead to a release of the positive bending moment at the beam mid span, which can be seen as beneficial for the fire performance of the beam. However, this negative bending moment at the beam end may also cause an increase in the bending moment at the column and be detrimental to the column's fire resistance. Therefore, in fire conditions, the relative restraints provided by the beam and column to each other are affected by the development and direction of the bending moment at the joint.

3.3 Working mechanism

Redistributions of internal forces may occur within the frame between the beam and column as temperature rises, which are mainly due to 1) the structural continuity of the frame, i.e. the deformations of the beam and column are restrained by each other and should be coordinated with each other; and 2) the differential thermal expansion and material degradations within the frame due to the non-uniform temperature distribution. To reveal the working mechanism of the TRC frame exposed to fire, the development during heating of the axial forces and bending moments at the mid-span and joint sections of the beam and the column section of the largest lateral deformation is analysed. Fig. 14 shows the FEA results of an example frame with n = 0.5 and m = 0.5.

Fig. 14(a) illustrates the axial force of the column during heating and the force proportions born by the concrete core, steel tube and rebars. Since the steel tube is designed not to sustain the axial load directly and its material properties degrade quickly as temperature rises, the axial force of the tube is very small and could generally be ignored. Consistent with the previous conclusions drawn on pin-ended TRC columns [2, 16], the axial force N_c of the column in a frame mainly redistributes among the steel rebars and concrete core. As the temperature increases, the axial force taken by the concrete core first decreases and then increases slightly, whereas the axial force in the rebars develops in an opposite pattern. The reasoning behind this axial load redistribution is related to several complex issues, i.e. differential thermal stress, differential material property degradation, and the combined effects of axial compression and second-order effect [2, 16]. It should be noted that in fire conditions, the axial deformation behaviour of a TRC framed column observed in Fig. 12 and the load redistribution within the composite section largely differ from those of the CFST framed columns reported by Han et al. [36-38]. These differences in the column behaviour further lead to the different overall performances and working mechanisms between these two types of composite frames exposed to fire.

Since the axial thermal expansion of the RC beam is restrained by the TRC column via the joint, an axial force is generated in the beam. The evolution during heating of the axial force

N_b in the beam is shown in Fig. 14(b). During the initial heating stage, the temperature of the beam increases at a very fast rate and the beam expands in the axial direction, causing the axial compressive force to increase significantly. As heating proceeds, the material properties of the rebars and concrete in the RC beam degrade continually. Consequently, the flexural stiffness of the beam decreases significantly, resulting in a continual increase of the flexural deflection. The inwards movement of the beam ends due to the flexural deflection would be restrained by the TRC columns and generates axial tension in the beam. As the beam deflects further, the catenary action may even occur in the beam [36-38]. The increasing flexural deflection and the occurrence of the catenary action cause the axial compressive force in the beam to decrease and even to turn into tension. It should be noted that the catenary action observed in the beam is highly related to the restraint level at the beam ends and the structural integrity of the frame and it considerably contributes to the load-bearing capacity of the beam in fire at the high-temperature phase. At the same time, the beam acting as a catenary pulling the TRC columns inwards induces further lateral deformation and bending moment of the columns, which could cause the columns and/or the joints to fail and eventually lead to an overall collapse of the frame.

The development over time of the bending moments of the column and beam is presented in Fig. 14(c). As expected, the mid span of the beam and the column section of the largest lateral deformation are subject to positive bending moments after ambient-temperature loading, whereas the joint section of the beam is subject to negative (hogging) bending moment. As heating progresses, the restrained differential thermal expansion generates axial compression in the lower section of the beam, whereas the upper part is in tension, forming a negative bending moment in the beam section. In the initial heating stage (around 1/3 of the whole heating duration), the thermal gradient within the beam section is particularly large due to the high heating rate. As a result, the negative bending moment due to differential thermal stresses is large and increases further as temperature rises. For the mid span of the beam, since the heat-induced negative bending moment counteracts the positive bending moment induced by the ambient-temperature loading, the total bending moment M_{bm} first decreases continually and even turns into negative. As heating carries on, the temperature gradient

decreases and the positive bending moment causing the flexural deflection dominates the behaviour of the beam. Thus, M_{bm} increases and becomes positive again. The bending moment M_{bj} at the joint section of the beam is the sum of M_{bm}, the bending moment caused by the applied UDL q_b and the second-order moment induced by the axial force N_b, of which M_{bm} dominates. Therefore, M_{bj} develops in a similar trend as for M_{bm}.

The TRC column in the frame is subject to the combined effects of the applied load N_f and the forces and bending moments transferred from the beam through the joint. As illustrated in Fig. 13(b), the bending moment M_c at the column section of the largest lateral deformation is the sum of M_{bj}, the moment induced by N_b and the second-order moment caused by N_f. The positive second-order moment is proportional to the lateral deformation of the column and increases continually during heating. The development of the bending moment induced by N_b follows the same trend as N_b. Generally, the moment M_{bj} transferred from the beam and the second-order moment induced by N_f are the two dominant components of the total bending moment M_c, whose development trends are opposite to each other in some stages as detailed above. Under the combined effects of all these complicated bending moment components, M_c first increases gradually and then decreases slightly until failure.

3.4 Development of axial stress

The development of axial stresses in the beam and column is closely affected by the axial force, bending moment, second-order effect, and the differential thermal expansion and differential material degradations caused by non-uniform temperature distribution. To further understand the fire behaviour of TRC frames, the axial stress distribution and development in the columns and beam are analysed in this section. The frame with $n = 0.5$ and $m = 0.5$ is again investigated as a typical example. The axial stress vs. time relationships of the concrete and rebars at representative positions in the column section of the largest lateral deformation and the mid span of the beam are shown in Fig. 15. The negative value in this figure indicates axial compression. The stress in the steel tube of the TRC column is not analysed as the tube hardly bears any axial load directly.

3.4.1 Stress in the column section of the largest lateral deformation

As shown in Fig. 15(a), the axial compressive stress in the concrete section induced by the ambient-temperature loading distributes linearly along the neutral axis of bending due to the second-order effect, as the plane section remains plane. The development of axial stresses at different locations in the concrete section (i.e. P1 to P5 in Fig. 15(a)) generally consists of two phases. In the first phase, the axial stresses are mainly affected by the differential thermal stresses due to restrained and non-uniform thermal expansion. In particular, the outer layers of the section (P1 and P5) are under compression and Points P2 to P4 are under tension. As heating progresses, the second phase starts, when the effect of the differential thermal stresses becomes insignificant as the sectional temperature gradient reduces. Also, the strength and stiffness of the outer concrete layers degrade significantly and the axial force in the column is gradually transferred to the inner concrete layers where the temperature is still relatively low. The axial compressive stresses in the column rebars (Rebar1 to Rebar5 in Fig. 15(b)) develop following a similar trend, i.e. an initial increase phase followed by a yielding phase and a final descending phase. The initial increase phase is mainly attributed to the effect of the thermal stresses, since the rebars are of higher thermal expansion coefficient than the surrounding concrete and are subject to compression due to restrained thermal expansion. Both the yield strength and elastic modulus of the rebars degrade significantly as temperature increases and thus the compressive stresses in the rebars decrease continually after yielding with the axial force born by the rebars being gradually transferred to the inner concrete, corresponding to the final descending phase.

3.4.2 Stress in the mid span of the beam

The neutral axis of bending of the T-shaped RC beam is initially located within the web of the section. As shown in Figs. 15(c) and 15(d), concrete Points P1 to P3 and Rebars 1-4 below the neutral axis are in tension due to the ambient-temperature loading, whereas P4, P5 and Rebar 5 are in compression. The development of the axial stresses in the concrete is mainly affected by the bending moments induced by the applied load and thermal stresses due to

restrained differential thermal expansion. For Points P1 to P4, in the initial heating stage, the thermal stresses (compressive) are dominant and their increase results in the continual increase of the total axial compressive stresses. As heating progresses, the influence of the differential thermal stresses decreases as the temperature gradient becomes insignificant, and the effect of material degradation becomes dominant. With the continual development of flexural deflection and the occurrence of the catenary action in the beam, the compressive stresses in Points P1-P4 decrease to very close to zero or even turn to tension (very low stress levels due to their very high temperatures and low tensile strengths) at failure. The axial stress at Point P5 is first mainly affected by the thermal stresses (tensile) and then dominated by the increasing flexural deflection and catenary action. The developments of the axial stresses at Rebars 1, 2 and 4 mainly include three phases. During the initial heating phase, the axial tensile stress undergoes a slight increase. In the second phase, as temperature increases, the axial stress turns into compression due to the restrained differential thermal expansion. Afterwards, the axial compressive stresses in these rebars decrease continually as the beam deflects further. The axial stress in Rebar 5 first turns from compression into tension due to the thermal stress (tensile) and then reverses to compression since the flexural deflection of the beam dominates. Throughout the heating process, the axial stress in Rebar 3 remains in tension, since it is dominated by the thermal stress (tensile) because its temperature is significantly lower than those of Rebars 1 and 4. The slight decrease of axial tensile stress is mainly due to the high-temperature strength degradation.

4. Effects of key parameters

4.1 Effect of joint-zone steel tube thickness

As noted in Section 3, a default thickness of 10 mm is used for the steel tube in the joint zone, following the minimum requirements for TRC joints in JGJ/T471 [13]. As the tube thickness may vary in engineering practices, studies are conducted to investigate the influences of the joint-zone steel tube thickness t_j (4.5, 10, 20 and 30 mm) on the high-temperature deformations of TRC columns and RC beams, by taking a frame with $\lambda = 30$, $n = 0.5$ and m

= 0.5 as an example. Fig. 16 shows the development of the axial deformation at column top and that of the flexural deflection at beam mid span during heating. The increase of the joint-zone steel tube thickness generally leads to slight decreases in the deformations of the beam and columns and an increase in the fire resistance of the whole frame. Although the joint-zone steel tube thickness may affect the local mechanical performance of the joint, its influence on the overall behaviour of the frame is relatively limited. Therefore, the default value (10 mm) of t_j that used in Section 3 is also adopted in the following analysis.

4.2 Effect of column load ratio on deformations and bending moments

Fig. 17 presents the influence of the column load ratio n (0.5, 0.6 and 0.7) on the axial deformation at the column top, the flexural deflection at the beam mid span and the bending moments along the beam and columns. For the frames investigated in Fig. 17, the column slenderness ratio is 30 and the beam load ratio is 0.5. In all cases, the columns experience axial contraction only throughout the entire heating duration, as shown in Fig. 17(a). As the column load ratio increases, the deformations of the beam and columns increase significantly. The failure modes of all cases are identical, which is the runaway of the axial deformation of the column, i.e. global buckling caused by uncontrolled overall deformation, as marked with the red dots in Fig. 17(a). As expected, the fire resistance of the frame decreases significantly as the column load ratio increases. As shown in Figs. 17(b)-17(d), the column load ratio hardly affects the developing patterns of the bending moments of the columns and beam. The developments of the positive moment M_{bm} at the beam mid span, the negative moment M_{bj} at the joint zone of the beam and the positive moment M_c at the column section of the largest lateral deformation are the same as detailed in Section 3.3 and hence not repeated here. The influences of the column load ratio on the initial bending moments of the beam and columns are marginal. The main reason is that the initial lateral deformation of the column due to the ambient-temperature loading and the corresponding bending moment due to second-order effect are little. As widely recognized, both the bending moment and flexural deflection at the mid span of a beam are negatively correlated to the supporting levels at the beam ends. Specifically, the mid-span bending moment and deflection of a beam under UDL increase

significantly as the rigidity of the beam end decreases. For the frames investigated in this study, as the column load ratio increases, the global axial and lateral deformations of the TRC column increase, leading that the relative supporting effect provided by the column to the beam decreases. Therefore, the increase of the column load ratio causes noticeable increases in the flexural deflection and bending moment at the beam mid span, as presented in Figs. 17(a) and 17(b). This in turn leads to a decrease of the joint bending moment M_{bj} in the beam as the applied load onto the beam remains constant during heating. This also causes the total bending moment M_c at the column section of the largest lateral deformation to decrease, because the bending moment transferred from the beam through the joint to the column decreases.

4.3 Effect of beam load ratio on deformations and bending moments

The influences of the beam load ratio m (0.3, 0.5 and 0.7) on the deformations and bending moments of the beam and columns in the frames of $\lambda = 30$ and $n = 0.5$ are shown in Fig. 18. For the cases with various beam load ratios, the evolution over heating of the axial deformations at column top end and that of the flexural deflections at beam mid span follow the same patterns (i.e. shape of curves) as observed from the frames of various column load ratios investigated in Fig. 17(a). Fig. 18(a) shows that as the beam load ratio increases, the flexural deflection at beam mid span increases significantly as expected; the axial deformation at column top end also increases but only very slightly, as the column load ratio remains unchanged here. The failure mode of all cases is the uncontrolled increase in the axial deformation of the column. The red dots in Fig. 18(a) illustrate the fire resistance (failure) time. The increase of the beam load ratio leads to a decrease in the fire resistance of the frame, whereas this negative effect is relatively limited. The beam load ratio is found to hardly affect the development trends of the bending moments in the beam and columns. These trends, as shown in Figs. 18(b)-18(d), are consistent with those discussed in Figs. 14 and 17. However, as the beam load ratio increases, the magnitudes of the bending moments of the beam and columns both increase during both the ambient-temperature loading and the subsequent heating stages. This effect is especially significant for the bending moments in

the beam.

4.4 Combined effect of column load ratio and beam load ratio on the overall fire resistance of the frame

The fire resistances of the frames of different column load ratios and beam load ratios are shown in Fig. 19. With the increase in either column load ratio or beam load ratio, the fire resistance of the frame decreases almost linearly. As observed from Figs. 17-19, the influences of the column load ratio on the deformations of the beam and columns and the fire resistance of the frame are larger than those of the beam load ratio. Two main reasons for this are: 1) the composite frame fails in fire mainly due to the runaway of the column axial deformation and the increase in column load ratio directly affects the axial force, bending moment and deformations of the columns; 2) the increase in the column load ratio could further affect the internal forces and flexural deflection of the RC beam, whereas increasing beam load ratio mainly affects the mechanical responses of the beam itself and its influence on the column is limited.

5. Fire resistance design recommendations

The structural fire resistance design of columns within composite frames is a complicated issue, as their fire performance is affected by various aspects, such as the frame type, the location of the fire and the load ratios of the beam and column. Consequently, close form solutions for the fire resistance design of steel-concrete composite columns that do not treat the columns as isolated members and account for the overall frame continuity are still very limited. To the authors' best knowledge, among the current fire design provisions of composite columns all over the world [13, 33, 43-46], only the Eurocode EC4 [33] gives some consideration to the effect of the rotational restraints at the ends of composite columns (via buckling length ratios).

Apart from the rotational restraints at the column ends, the fire behaviour of TRC columns in a frame is also highly affected by the axial restraints to thermal expansion, bending

moments transferred from the connected beams and the behaviour of joints, etc. Therefore, the approach given in EC4 [33] may be over simplified and cannot account for the real behaviour of a composite frame.

This section aims to propose a practical fire design method for square TRC columns within a composite frame. The fire resistance design methods of pin-ended and end-restrained square TRC columns that previously developed by the authors [15, 16, 23] are used as a basis for this development. The fire behaviour of TRC columns in a frame and that of isolated TRC columns with end restraints are compared. Eventually, a fire resistance design method for square TRC columns in composite frames is developed, by quantifying the difference between the fire resistance of framed columns and isolated columns.

5.1 Fire resistance design of isolated TRC columns – a brief reminder

As presented in Fig. 20(a), the pin-ended TRC columns are considered to reach their fire resistance $t_{FR,p}$ when their high-temperature buckling resistance $N_{b,T}$ (i.e. the compressive resistance $N_{u,T}$ multiplied by the reduction coefficient φ_T) falls below the applied axial load N_f. The compressive resistance $N_{u,T}$ is related to the high-temperature material properties (e.g. compressive strength, modulus of elasticity and yield strength) of the concrete and steel. The buckling curve (c) given in EC4 [33] and the buckling curve for square TRC columns given in JGJ/T471 [13] are recommended for the determination of φ_T.

Figs. 20(b) and 20(c) illustrate the reasons for the axial and rotational restraints to be beneficial for the fire resistance of square TRC columns [23]. For the axially-restrained column, part of the applied load N_f at the column top is gradually transferred to the adjacent restraining structures during heating, causing a continual decrease of the axial force inside the TRC column. The restrained column fails at time $t_{FR,a}$ when $N_{b,T}$ degrades to the axial force of the column rather than the initially-applied load N_f. The failure axial force N_{af} of the column with axial restraints is a function of the axial force ratio n_f (the ratio between N_{af} and the column's buckling resistance at ambient temperature) at failure. Compared to pin-ended columns, the high-temperature buckling length ratio μ_f of the column with rotational restraints is smaller, causing the buckling resistance of restrained columns to decrease more

slowly with heating and causing the fire resistance $t_{FR,r}$ of a restrained column to be higher than that of the equivalent unrestrained column.

For square TRC columns with axial restraint ratio α and rotational restraint ratio β, the detailed design equations proposed in reference [23] to determine $N_{b,T}$ and N_{af} at an arbitrary heating time t are listed below as Eqs. (1) – (14). It should be noted that when both α and β are equal to zero, these design equations (1) – (14) for restrained columns are the same as those proposed for pin-ended columns [15].

$$N_{af} = N_f n_f / n \tag{1}$$

$$n_f = n - f(\beta)(3.6 - 0.047\lambda)\alpha \tag{2}$$

$$N_{b,T} = \varphi_T N_{u,T} \tag{3}$$

$$N_{u,T} = (f_{c,eq,T} + 5.1 f_{el,T}) A_c + k_{bT} f_b A_b \tag{4}$$

$$f_{c,eq,T} = \frac{1 - (\frac{0.045}{B_c} - 0.016)t}{1 + (0.0054t + 0.22)\sqrt{\frac{t}{B_c}}} f_c' \tag{5}$$

$$f_{el,T} = \frac{1.5 k_{s,T} t_s k_{yT} f_y}{B} \tag{6}$$

$$k_{s,T} = \frac{27 t_s}{B}\sqrt{\frac{k_{yT} f_y}{235}}\left(\frac{30}{f_{c,eq,T}}\right) \tag{7}$$

$$\varphi_T = \frac{1}{\Phi + \sqrt{\Phi^2 - \overline{\lambda}_T^{\,2}}} \quad \text{(EC4)} \qquad \text{or}$$

$$\varphi_T = \begin{cases} 1 & \overline{\lambda}_T \le 0.15 \\ \left[1 + (1+\varepsilon_1)/\overline{\lambda}_T^{\,2}\right]/2 - \sqrt{\left[1 + (1+\varepsilon_1)/\overline{\lambda}_T^{\,2}\right]^2/4 - 1/\overline{\lambda}_T^{\,2}} & 0.15 \le \overline{\lambda}_T \le 1 \quad \text{(JGJ/T471)} \\ \left[1 + (1+\varepsilon_2)/\overline{\lambda}_T^{\,2}\right]/2 - \sqrt{\left[1 + (1+\varepsilon_2)/\overline{\lambda}_T^{\,2}\right]^2/4 - 1/\overline{\lambda}_T^{\,2}} & \overline{\lambda}_T \ge 1 \end{cases} \tag{8}$$

$$\overline{\lambda}_T = \sqrt{\frac{N_{u,T}}{N_{cr,T}}} \tag{9}$$

$$N_{cr,T} = \frac{\pi^2 (EI)_{fi,eff}}{L_{eff}^{\,2}} \tag{10}$$

$$(EI)_{fi,eff} = k_{sET} E_s I_s + k_{bET} E_b I_b + C k_{cET} E_c I_c \tag{11}$$

$$k_{cET}=\frac{2636\left[1-(\frac{0.045}{B_c}-0.016)t\right]}{2500+\left[6\cdot(\frac{-9.8t^2+92.7t}{B_c}+20)+0.04\cdot(\frac{-9.8t^2+92.7t}{B_c}+20)^2\right]} \quad (12)$$

$$L_{eff}=\mu_f L \quad (13)$$

$$\mu_f=\frac{1+0.41\beta_t}{1+0.82\beta_t} \quad (14)$$

where k_{yT} and k_{sET} are the reduction coefficients of the yield strength and elastic modulus of the steel tube at temperature T_s ($T_s=1080-450\exp(-0.8t)-630\exp(-3t)+20$), respectively; k_{bT} and k_{bET} are the corresponding reduction coefficients of the rebars at temperature T_b ($T_b=(T_s-20)\exp\left\{\left(\frac{13.5(2x/B_c-1)}{(0.36t/B_c^2)^{3/4}}\right)\left(1-1.5\left(\frac{2y}{B_c}\right)^2\left(1-\frac{2x}{B_c}\right)\right)\right\}+20$). These four reduction coefficients could be determined based on the tabulated values given in EC4 [33];

t (in hours) is the heating time of the ISO 834 standard fire [26];

B, B_c and t_s (both in metres) are the outer and inner widths and wall thickness of the steel tube, respectively;

C is a coefficient to account for the sectional stiffness reduction of concrete and $C=0.6+2\frac{\alpha_s+\rho}{1+\alpha_s+\rho}\le 0.9$;

$f(\beta)=\begin{cases}16\beta+1 & \beta\le 0.05\\ 1.8 & \beta>0.05\end{cases}$, $\beta_t=(60a_{n,B}t+1)\beta$, $a_{n,B}=0.094/B+n-0.46$.

The stiffnesses of the end restraints may become temperature-dependent when the surrounding members are also exposed to fire. Fig. 21(a) summarises the comparison between the FEA simulated [23] fire resistances of square TRC columns with temperature-dependent restraints (TDR) and those of the constant restraints (CR). When altering the end restraint from constant to temperature-dependent, the fire resistance of TRC columns generally decreases by a magnitude within 10% [23]. Therefore, it is recommended for the fire resistance of a TRC column with TDR to be the fire resistance of the column with CR multiplied with a reduction factor of 0.9. As shown in Fig. 21(b), this design recommendation generally yields a good prediction for the fire resistance of square TRC columns with TDR.

5.2 Comparison of the fire behaviour between the framed and isolated TRC columns

FEA modelling is conducted in this section to study the difference between the high-temperature behaviour, in particular, overall deformations, axial forces and bending moments, of square TRC columns in a frame and those of isolated columns. Isolated columns refer to the columns with fixed bottom end and pinned or restrained top end. Since the single-storey and single-span frame investigated in this study is symmetric in plane, the restraints provided by the RC beam to the column top end are mainly rotational, which are modelled by rotational springs in ABAQUS. Since the RC beam is also exposed to fire, the rotational restraint at the top end of the column in a frame is temperature-dependent, which is adopted in the models. In addition, given that this section aims to develop a practical design method, the simplification of assuming the end stiffness being constant over heating is also investigated. The determination of the temperature-dependent stiffness has been previously proposed by the authors and is described in detail in reference [23] and thus not repeated here. For the constant stiffness cases, the ambient-temperature stiffness of the joint zone, which is the initial slope of the FEA simulated bending moment–rotation curve, is adopted and assumed to remain constant during heating. To enable comparison, the loading (axial force, shear force and bending moment) applied onto the isolated columns is equivalent to those generated within the frame.

Fig. 22 presents the development over time of the axial deformation at column top, lateral deformation, axial force and bending moment at the section of the largest lateral deformation in the framed column and isolated columns with constant restraint, temperature-dependent restraint and pinned end conditions. The investigated columns in Fig. 22 are with $\lambda = 30$, $n = 0.5$ and $m = 0.5$. As shown in Fig. 22(a), the axial deformations of the columns of different top-end conditions are identical before runaway, indicating that the rotational restraint hardly affects the axial deformation of the column. Fig. 22(b) shows that the axial forces of the TRC columns of different top restraints remain constant during heating, confirming that it is reasonable to simplify the restraints at the top end of the column as rotational only. As

presented in Fig. 22(c), the lateral deformation of the framed column is significantly larger than those of the isolated columns, which is mainly due to the outward push induced by the thermal expansion of the connected RC beam. Compared to the pin-ended column, the column end rotational restraint results in a decrease in the lateral deformation of the column. When altering the top end restraint from constant to temperature-dependent, the lateral deformation of the column increases very slightly. Fig. 22(d) shows that the bending moments at the sections of the largest lateral deformation of the isolated columns with different top end restraints develop in a similar pattern, i.e. increasing continually before failure. This is very different from that observed from the framed column, as detailed in Section 3.3. The bending moment of the framed column is far larger than those of the isolated columns with or without end restraints. This is mainly attributed to 1) among the four investigated cases, the lateral deformation and the corresponding second-order moment induced by the axial force in the framed column is the largest; 2) the flexural deflection, axial expansion, axial force and bending moment in the RC beam may also increase the bending moment in the framed column. The FEA simulated fire resistances for the pinned-fixed column, CR-fixed column, TDR-fixed column and frame-fixed column are 222.8 min, 278.8 min, 268.7 min and 251.3 min, respectively. The buckling length ratio of a column is usually defined as the ratio between the buckling length and the whole length of the column. Yang et al. [23] recommend using the zero-moment method, i.e. measuring the distance between the zero points of the bending moment diagrams extracted from FEA, to determine the buckling length of a TRC column at the fire limit state. The corresponding buckling length ratios of these columns at failure, which are determined by this zero-moment method [23], are 0.69, 0.56, 0.59 and 0.61, respectively. Both the fire resistance and the buckling length ratio of the framed column lie between those of the pin-ended column and the TDR column.

The column with its bottom end fixed and top end integrated into a single-storey and single-span frame could be seen as equivalent to a column on the top floor of a multi-storey frame when compartment fire is considered. As mentioned above, the FEA calculated high-temperature buckling length ratio of the TRC column of such end conditions in a frame is 0.61. On the other side, EC4 [33] recommends that the buckling length ratio of a column

with such end conditions is 0.7, which is the same as that predicted by the authors [23] from isolated TRC columns with pinned-fixed boundary conditions.

Fig. 23 shows the comparison between the fire resistance of TRC columns in a frame and those of equivalent isolated columns. All columns are of λ = 30 and 50, n = 0.5, 0.6 and 0.7 and m = 0.3, 0.5 and 0.7. With the increase in load ratio of either the column or beam, the fire resistances of all columns decrease almost linearly. The fire resistance of the isolated columns of constant restraint (CR) is the largest, with those of the isolated columns of temperature-dependent restraint (TDR), framed column and pin-ended column are in descending order. As mentioned above, the effects of the frame continuity on the fire resistance of the TRC columns generally involve two opposite aspects. The RC beam not only provides rotational restraint to the TRC column, but also increases the lateral deformation and bending moment of the column. The fire resistance of the framed column is higher than that of the pin-ended column, indicating the beneficial effect provided by the beam dominates over the negative effect. Given that simplifying the restraints provided by the RC beam with rotational springs does not account for the above-mentioned unfavourable effect, the fire resistance of the framed column is lower than that of the TDR column. Consistent with the conclusions drawn for rotationally-restrained isolated TRC columns [23], the higher the slenderness ratio of the column, the larger the overall beneficial effect of the frame continuity on the fire resistance of the column. For instance, when λ = 30, the average ratio between the fire resistance of the framed column and that of the pin-ended column is 1.27. As the slenderness ratio increases to 50, this ratio increases to 1.77.

5.3 Design recommendations of TRC columns in a frame

Fig. 24 summarises the FEA simulated fire resistance of the framed columns with various column slenderness ratios, column load ratios and beam load ratios, compared with the equivalent bottom-fixed isolated columns. The average ratios between the fire resistance of the framed column and those of isolated columns with various top end restraints (pinned, temperature-dependent and constant) are 1.56, 0.88 and 0.8, respectively. The three solid lines in Fig. 24 correspond to the fire resistance of the pin-ended column, 0.85 times of the

fire resistance of the TDR column and 0.75 times of the fire resistance of the CR column, respectively. Considering both safety and practicality, it is suggested to design the fire resistance of a TRC column in a single storey frame or on the top floor of a multi-storey frame as 0.75 times of that of an equivalent isolated column of constant restraint on one end and fixed on the other end.

Fig. 25(a) shows the comparison between the FEA simulated fire resistances of square TRC columns with constant rotational restraints at their top ends and the fire resistances determined using the design formulae proposed by the authors for isolated square TRC columns with end restraints [23]. When the EC4 buckling curve (c) is used for calculating the reduction coefficient, the average ratio between the formula calculated and the FEA simulated fire resistances is 0.96, with a standard deviation of 0.09. As for the case of adopting the buckling curve given in JGJ/T471, the corresponding results are 0.94 and 0.08. To further validate the above-proposed simplified design formula, more numerical examples of framed TRC columns with various parameters, e.g. concrete compressive strength (30 MPa to 60 MPa), rebar yield strength (300 MPa to 500 MPa), steel tube yield strength (235 MPa to 460 MPa), steel ratio (2% to 6%), reinforcement ratio (2% to 6%), column slenderness ratio (30 to 60) and load ratio (0.3 to 0.7), are calculated. The fire resistance of the framed columns given by FEA and 0.75 times of the formula calculated fire resistance of the equivalent columns with constant rotational restraints at their top ends is compared in Fig. 25(b). An average ratio of 0.94 and a standard deviation of 0.24 are achieved for this comparison by using the EC4 buckling curve (c) to determine the reduction coefficient. When the buckling curve given in JGJ/T471 is used, the average ratio is 0.92 with a standard deviation of 0.23. Considering the complexity of the fire performance of columns in a frame, it could be sufficient to use the previously-proposed design method for isolated columns with end restraints [23], multiplied with a reduction factor of 0.75 to determine the fire resistance of square TRC columns in a frame. For the comparison purpose, Fig. 25(b) also compares the FEA calculated fire resistances of TRC framed columns with those predicted using the EC4 method, i.e. taking the effective length ratio of the column in fire as 0.7. To be consistent with the European design system, the EC4 buckling curve (c) is adopted for determining the

buckling reduction coefficient. Generally, the EC4 approach gives a safe but conservative prediction, achieving an average ratio of 0.78 between the predicted and modelled fire resistances.

It should be noted that the design recommendation proposed in this study is so far applicable to square TRC columns in single-storey and single-span frames or columns on the top floor of multi-storey frames. It is speculated that the design concept proposed in this study, i.e. designing the fire resistance of a framed column as that of the equivalent end-restrained isolated column multiplied with a reduction factor, may also be applicable to TRC columns on the intermediate floors of a frame. However, the reduction factor may not be 0.75 and needs to be determined via systematic analysis. This is mainly because the end conditions of a column on the intermediate floor are generally stronger than those of a column on the top floor. For instance, EC4 recommends a buckling length ratio of 0.5 for the heated columns on the intermediate floor of a composite frame, which is lower than the value of 0.7 for the column on the top floor.

As recognized, the direct research on the exposed multi-storey and multi-span frames is the most realistic approach to reveal the fire behaviour of TRC columns in real application cases, e.g. high-rise structures. However, as pointed out above, the fire performance analysis and design of multi-storey and multi-span TRC frames are very complicated issues. The study conducted in this paper forms an initial attempt at understanding the fire performance of TRC columns in composite frames, which contributes to the development of a relevant performance-based design method. Although the single-storey and single-span frame is not the real form of frames in engineering, it is the most basic unit of multi-storey and multi-span frames. Moreover, compartment fire without considering the vertical fire spread is commonly assumed in current structural fire design methodologies. In this condition, the fire performance design of a multi-storey and multi-span frame could be simplified to and concentrated on a one-storey and one-span case. Therefore, fire performance of single-storey and single-span composite frames has attracted the interest of researchers. For instance, as noted in Section 2.2.1, Han et al. [36-38] have conducted both experimental investigations and numerical simulations on the fire behaviour of single-storey and single-span CFST

columns. Conceptually, the general working mechanism of a TRC column in a multi-storey and multi-span frame exposed to fire is similar to that of a column in a single-storey and single-span frame. Thus, the qualitative conclusions drawn in Sections 3 and 4, such as the thermal response, failure mode, load redistribution within the column section, bending moment transfer between the beam and column through the joint and the influences of key parameters on the column fire resistance, may also be applicable to multi-storey and multi-span frames. However, different from the single-storey and single-span cases, the end restraints of TRC columns in multi-storey and multi-span frames include both rotational restraints and axial restraints provided by adjacent beams and columns. With reference to the design approach used in this study, the quantitative relationship between the fire resistance of the TRC framed columns in multi-storey and multi-span frames and that of the simplified end-restrained columns could be established. Whereas the specific reduction coefficient may not be 0.75, as the restraint stiffnesses from the surrounding members to the column ends become different. Further experimental and numerical work on TRC columns within a multi-storey and multi-span frame, e.g. in the intermediate storey and the lowest storey, is ongoing. Corresponding design methods, e.g. the exact reduction coefficients of fire resistance will be given in the future. The research methodology used in this paper could serve as the basis of these further studies.

6. Conclusions

This paper presents the FEA modelling and theoretical analysis on the fire behaviour of square TRC columns in single-storey and single-span non-sway frames. Based on the research work conducted in this study, the following conclusions could be drawn:

(1) The 3D FEA model developed in this study considers the nonlinearities of material, geometry and contacts. After validations against test results on CFST frames, this model could be used to predict the temperature distributions, overall deformations and failure modes of TRC columns in composite frames exposed to fire.

(2) The temperatures in the beam-to-column joint zone of the frame are lower than those in the non-joint zone. The overall deformations, axial stresses, redistributions of axial forces

and bending moments in the TRC columns and RC beam of the frame are highly affected by the applied loads, second-order effects, differential thermal stresses and material degradations.

(3) The failure of the composite frame is mainly caused by the uncontrolled increase of axial deformation at the column top end. With the increase of beam load ratio or column load ratio, the axial deformation of the column and the flexural deflection of the beam both increase and the fire resistance of the frame decreases approximately linearly. The column load ratio has a larger influence on the fire behaviour (e.g. fire resistance) of the frame than the beam load ratio. The influence of the thickness of the semi-continuous steel tube on the overall mechanical responses of the frame is limited.

(4) The composite frame could provide considerable rotational restraints to the TRC columns but also increase lateral deformation and bending moment of the column. The fire resistance of a TRC column in a single-storey and single-span frame lies between those of equivalent columns with pinned (lower bound) and rotationally restrained (upper bound) top ends and with fixed bottom ends.

(5) On the basis of the previously-proposed design methods for pin-ended and end-restrained columns, a practical fire design recommendation is developed for square TRC columns in single-storey frames. Specifically, it is suggested to design the fire resistance of a TRC column in a single storey frame or on the top floor of a multi-storey frame as 0.75 times of that of an equivalent isolated column of constant restraint on one end and fixed on the other end. Combining this and previous studies [15, 16, 23], fire resistance design methods have been developed for TRC columns with different end restraints, i.e. idealised pinned or fixed, predefined axial and rotational end restraints, and being integrated into a frame.

Acknowledgements

The research work in this paper is financially supported by the National Natural Science Foundation of China (51978209), to which the authors are grateful.

Reference

[1] Zhou X H, Liu J P. Performance and design of steel tube confined concrete members. Beijing, China: Science Press Ltd.; 2010 [in Chinese].

[2] Yang D D, Liu F Q, Huang S, Yang H. ISO 834 standard fire test and mechanism analysis of square tubed-reinforced-concrete columns. Journal of Constructional Steel Research, 2020, 175: 106316.

[3] Zhou X H, Liu J P. Application of steel-tubed concrete structures in high-rise buildings. International Journal of High-Rise Buildings, 2019, 8(3): 161–167.

[4] Tomii M, Sakino K, Watanabe K, Xiao Y. Lateral load capacity of reinforced concrete short columns confined by steel tube, Proceedings of the International Speciality Conference on Concrete Filled Steel Tubular Structures, Harbin, China (1985), 19–26.

[5] Aboutaha R S, Machado R I. Seismic resistance of steel-tubed high-strength reinforced-concrete columns. Journal of Structural Engineering, 1999, 125(5): 485–494.

[6] Lahlou K, Lachemi M, AÏtcin P C. Confined high-strength concrete under dynamic compressive loading. Journal of Structural Engineering, 1999, 125(10): 1100–1108.

[7] Sun Y P, Sakino K. Earthquake-resisting performance of RC columns confined by square steel tube, Part 3: effects of shear span ratio of column. Journal of Structural & Construction Engineering, AIJ, 2011, 547: 129–136.

[8] Han L H, Yao G H, Chen Z B, Yu Q. Experimental behaviours of steel tube confined concrete (STCC) columns. Steel and Composite Structures, 2005, 5(6): 459–484.

[9] Zhang S M, Liu J P. Seismic behavior and strength of square tube confined reinforced-concrete (STRC) columns. Journal of Constructional Steel Research, 2007, 63(9): 1194–1207.

[10] Wang X D, Liu J P, Zhang S M. Behavior of short circular tubed-reinforced-concrete columns subjected to eccentric compression. Engineering Structures, 2015, 105: 77–86.

[11] Li X, Liu J, Wang X, Dong B, Chen Y F. Hysteretic behavior of circular tubed reinforced concrete column to steel beam frames. Journal of Building Engineering, 2021. https://doi.org/10.1016/j.jobe.2021.103475.

[12] Li X, Liu J, Zhou X, Wang X, Chen Y F. Experimental and numerical investigations on

seismic behavior of circular tubed reinforced concrete column to RC beam frames. Earthquake Engineering & Structural Dynamics, 2022, 1–21. https://doi.org/10.1002/eqe.3612.

[13] JGJ/T471, Technical Standard for Steel Tube Confined Concrete Structures, MOHURD (Ministry of Housing and Urban-Rural Development of the People's Republic of China), Beijing, China, 2020 [In Chinese]

[14] Liu F Q, Wang Y Y, Gardner L, Varma A H. Experimental and numerical studies of reinforced concrete columns confined by circular steel tubes exposed to fire. Journal of Structural Engineering (ASCE), 2019, 145(11): 04019130.

[15] Yang D D, Liu F Q, Huang S, Yang H. Structural fire safety design of square and rectangular tubed-reinforced-concrete columns. Structures, 2021, 29: 1286–1321.

[16] Yang D D, Liu F Q, Huang S, Yang H. Fire performance of eccentrically-loaded square and rectangular tubed-reinforced-concrete columns. Structures, 2021, 33: 1053–1076.

[17] Liu F Q, Gardner L, Yang H. Post-fire behaviour of reinforced concrete stub columns confined by circular steel tubes. Journal of Constructional Steel Research, 2014, 102: 82–103.

[18] Yang H, Liu F Q, Gardner L. Post-fire behaviour of slender reinforced concrete columns confined by circular steel tubes. Thin-Walled Structures, 2015, 87: 12–29.

[19] Liu F Q, Yang H, Gardner L. Post-fire behaviour of eccentrically loaded reinforced concrete columns confined by circular tubes. Journal of Constructional Steel Research, 2016, 122: 495–510.

[20] Liu F Q, Yang H, Yan R, Wang W. Experimental and numerical study on behaviour of square steel tube confined reinforced concrete stub columns after fire exposure. Thin-Walled Structures, 2019, 139: 105–125.

[21] Liu F Q, Yang H, Wang W. Behaviours of concentrically and eccentrically loaded square steel tube confined reinforced concrete slender columns after fire exposure. Thin-Walled Structures, 2021, 158: 107155.

[22] Yang D D, Liu F Q, Yang H. Comparison on fire performance of circular and square steel tube confined reinforced concrete columns. Journal of Building Structures, 2018, 39(11): 65-73. [in Chinese]

[23] Yang D D, Liu F Q, Huang S, Yang H. Structural behaviour and design of end-restrained square tubed-reinforced-concrete columns exposed to fire. Journal of Constructional Steel Research, 2021, 182: 106675.

[24] EN 1992-1-1, Eurocode 2: Design of Concrete Structures - Part 1–1: General Rules and Rules for Buildings, European Committee for Standardization, Brussels, 2004.

[25] GB 50010-2010, Code for Design of Concrete Structures. MOHURD (Ministry of Housing and Urban-Rural Development of the People's Republic of China), Beijing, China, 2010 [In Chinese]

[26] ISO 834-1, Fire Resistance Test - Elements of Building Construction, Part 1: General Requirements, International Organization for Standardization ISO 834, Geneva, Switzerland, 1999.

[27] EN 1991-1-2, Eurocode 1: Actions on Structures- Part 1–2: General Actions-Actions on Structures Exposed to Fire, European Committee for Standardization, Brussels, 2002.

[28] Ding J, Wang Y C, Realistic modelling of thermal and structural behaviour of unprotected concrete filled tubular columns in fire. Journal of Constructional Steel Research, 2008, 64(10): 1086–1102.

[29] Lv X T, Yang H, Zhang S M, Effect of contact thermal resistance on temperature distributions of concrete-filled steel tubes in fire. Journal of Harbin Institute of Technology, 2011, 18(1): 81–88.

[30] Lie T T. Fire resistance of circular steel columns filled with bar-reinforced concrete. Journal of Structural Engineering, 1994, 120: 1489–1509.

[31] Han L H. Concrete filled steel tubular structures-theory and practice (third edition), Science Press, Beijing (China) (2016) [in Chinese]

[32] Hong S, Varma A H. Analytical modeling of the standard fire behavior of loaded CFT columns. Journal of Constructional Steel Research, 2009, 65: 54–69.

[33] EN 1994-1-2, Eurocode 4 - Design of Composite Steel and Concrete Structures - Part 1–2: General Rules - Structural Fire Design, CEN, Brussels, 2008.

[34] EN 1994-1-1, Eurocode 4 - Design of Composite Steel and Concrete Structures – Part 1-1: General Rules and Rules for Buildings, CEN, Brussels, 2004.

[35] Tao Z, Han L H, Uy B, Chen X. Post-fire bond between the steel tube and concrete in

concrete-filled steel tubular columns. Journal of Constructional Steel Research, 2011, 67: 484-496.

[36] Han L H, Song T Y, Zhou K. Fire safety design theory of steel-concrete composite structures (2rd edition). Beijing, China: Science Press Ltd.; 2017 [in Chinese].

[37] Han L H, Wang W H, Yu H X. Experimental behavior of reinforced concrete (RC) beam to concrete-filled steel tubular (CFST) column frames subjected to ISO-834 standard fire. Engineering Structures, 2010, 32(10): 3130–3144.

[38] Han L H, Wang W H, Yu H X. Analytical behaviour of RC beam to CFST column frames subjected to fire. Engineering Structures, 2012, 36: 394–410.

[39] Ding J, Wang Y C. Experimental study of structural fire behaviour of steel beam to concrete filled tubular column assemblies with different types of joints. Engineering Structures, 2007, 29: 3485–3502.

[40] Pires T A C, Rodrigues J P C, Silva J J P. Fire resistance of concrete filled circular hollow columns with restrained thermal elongation. Journal of Constructional Steel Research, 2012, 77: 82-94.

[41] Correia A J P M, Rodrigues J P C. Fire resistance of partially encased steel columns with restrained thermal elongation. Journal of Constructional Steel Research, 2011, 67(4): 593-601.

[42] A.H. Buchanan, A.K. Abu, Structural design for fire safety, John Wiley & Sons, New Zealand (2017) 124–126.

[43] GB 50017-2017, Code for design of steel structure, MOHURD (Ministry of Housing and Urban-Rural Development of the People's Republic of China), Beijing, China, 2018 [In Chinese]

[44] GB 50936, Technical Code for Concrete Filled Steel Tubular Structures, MOHURD (Ministry of Housing and Urban-Rural Development of the People’s Republic of China), Beijing, China, 2014 [In Chinese].

[45] AIJ, Recommendations for Design and Construction of Concrete-Filled Steel Tubular Structures, Architectural Institute of Japan, Tokyo, Japan, 2008 [In Japanese].

[46] ASCE/SEI/SFPE 29–05, Standard calculation methods for structural fire protection, ASCE, Reston, VA, 2007.

Figures

(a) Circular TRC columns used in Qingdao Haitian Centre [3]

(b) Rectangular TRC columns used in China Resources Xiaojing Bay Hotel

Fig. 1. Typical applications of TRC columns in engineering practices.

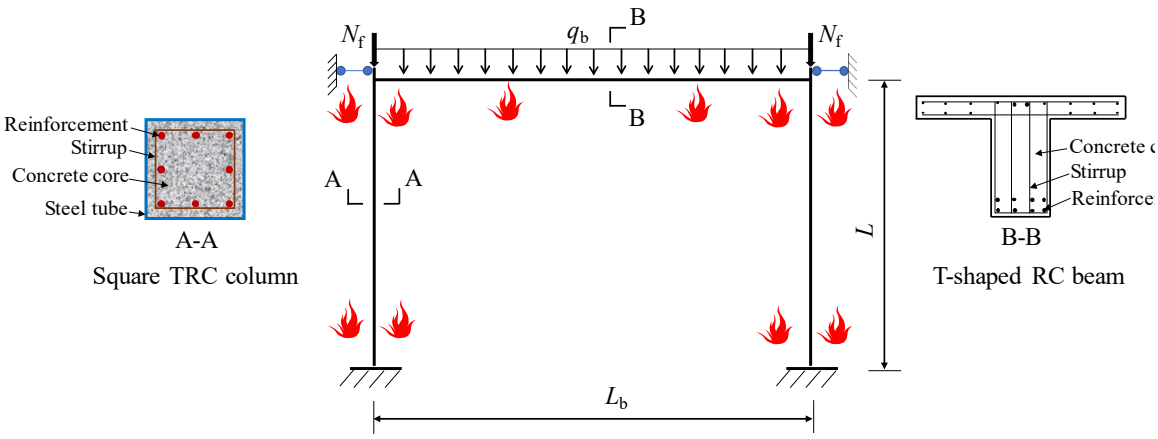

Fig. 2. Schematic of the square TRC column-RC beam frame.

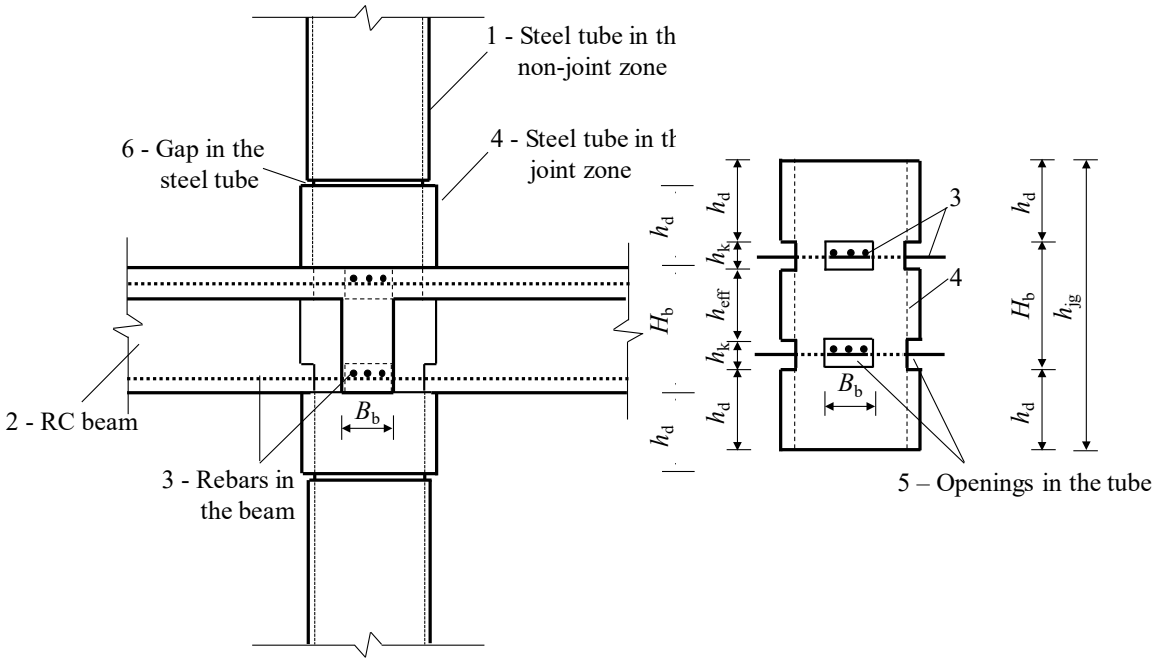

(a) Semi-continuous joint (b) Openings in steel tube in the joint

Fig. 3. Illustration of the semi-continuous joint used in TRC column-RC beam frames [13].

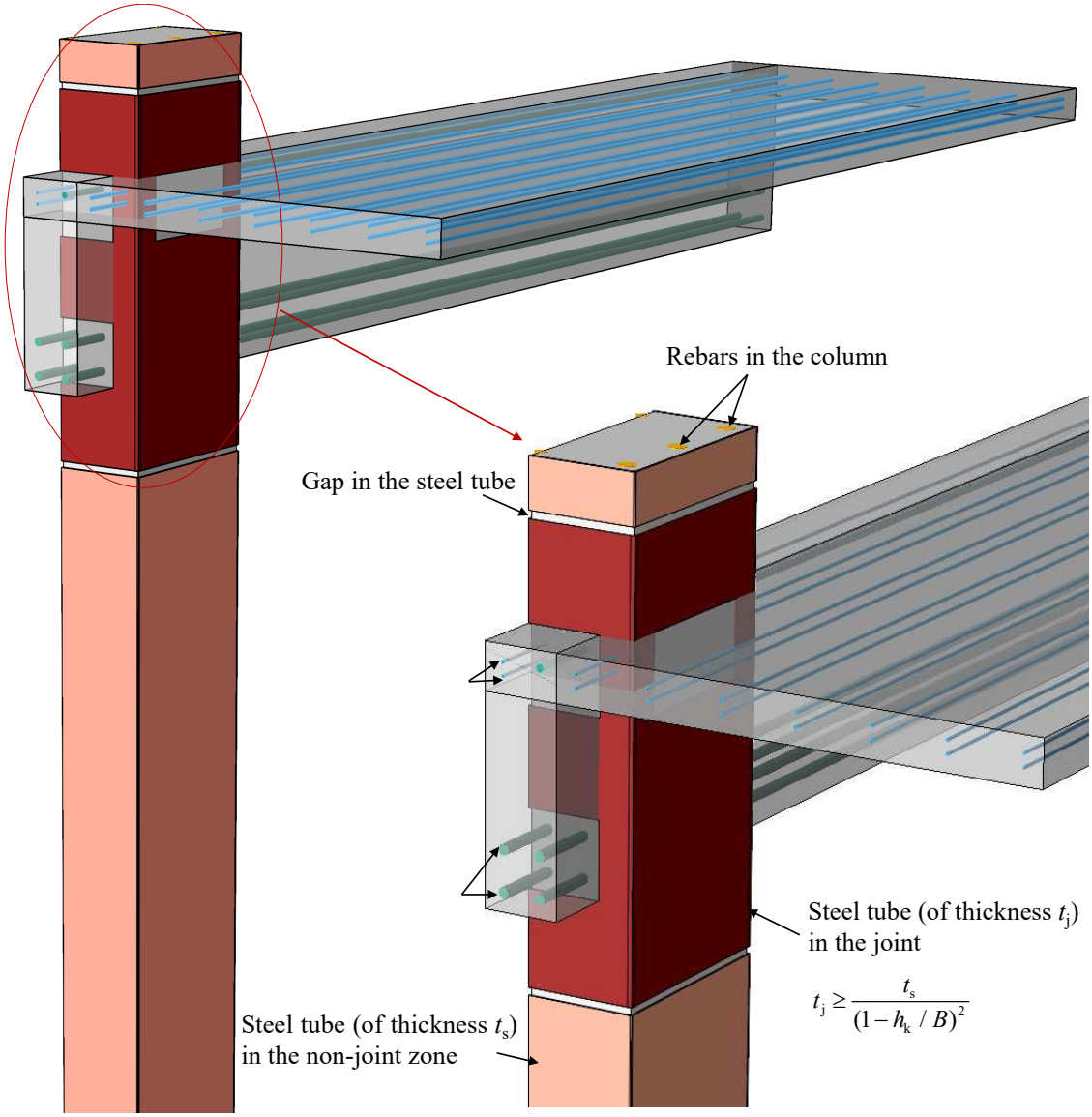

Fig. 4. Details of the square TRC column-RC beam frame built in FEA modelling.

(a) Failure mode of frame CFRC-1

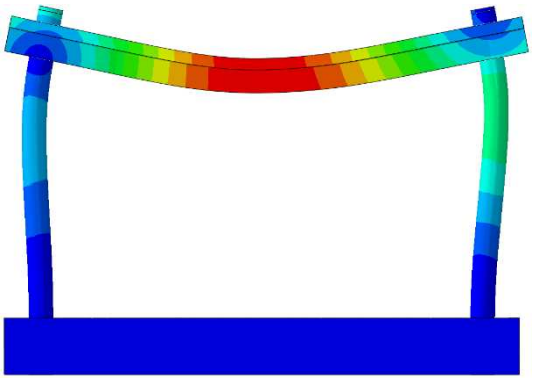

(b) Predicted failure mode of frame CFRC-1

(c) Failure mode of frame SFRC-1

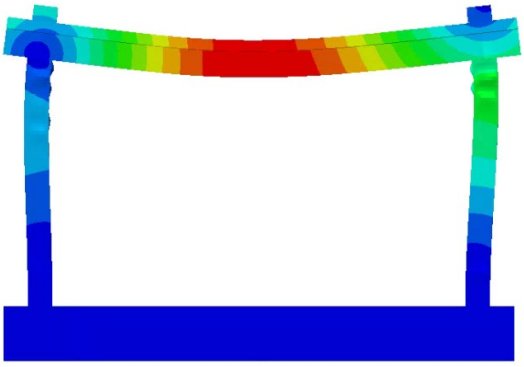

(d) Predicted failure mode of frame SFRC-1

Fig. 5. Comparison between the experimental and simulated failure modes of CFST frames [37].

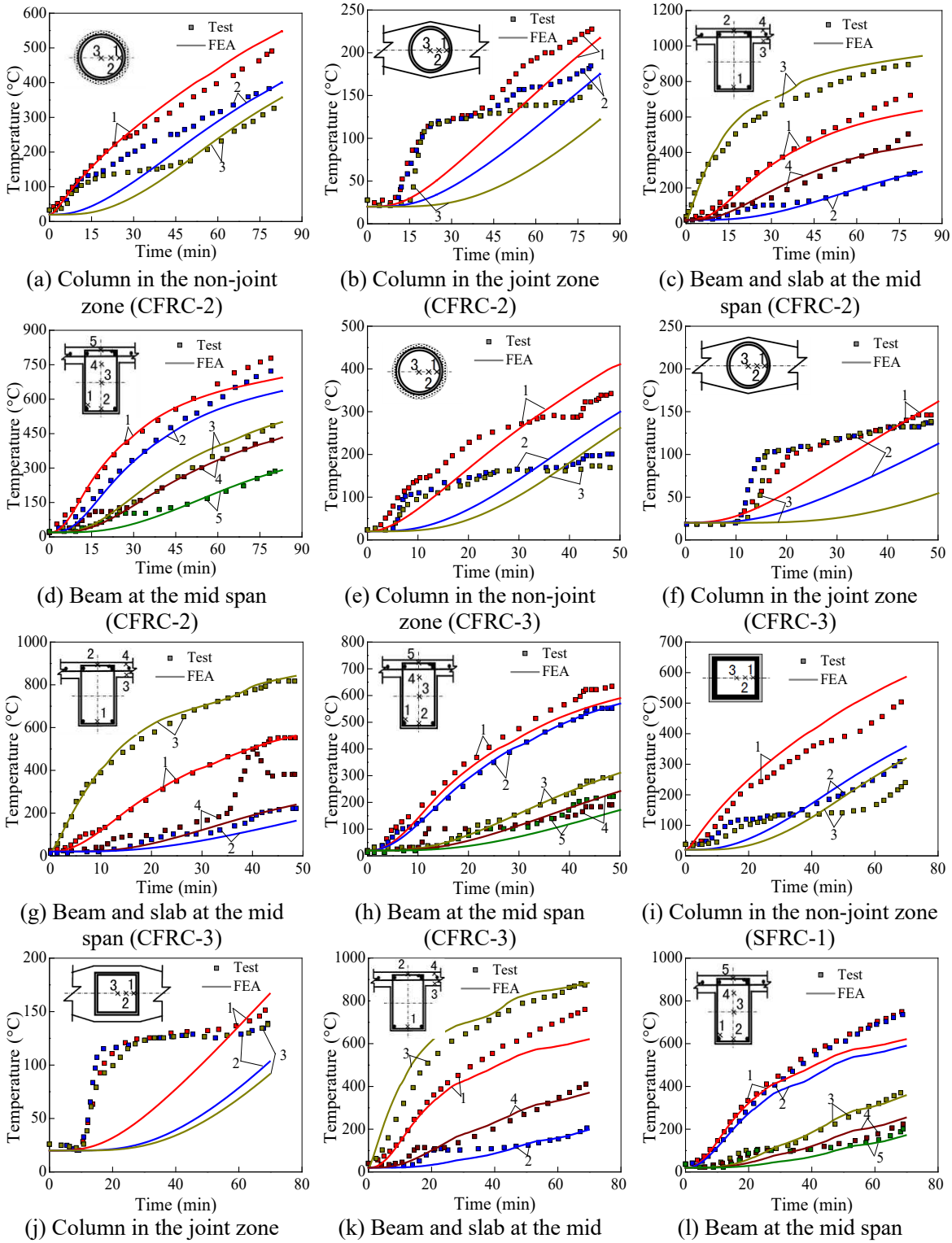

(a) Column in the non-joint zone (CFRC-2)
(b) Column in the joint zone (CFRC-2)
(c) Beam and slab at the mid span (CFRC-2)
(d) Beam at the mid span (CFRC-2)
(e) Column in the non-joint zone (CFRC-3)
(f) Column in the joint zone (CFRC-3)
(g) Beam and slab at the mid span (CFRC-3)
(h) Beam at the mid span (CFRC-3)
(i) Column in the non-joint zone (SFRC-1)
(j) Column in the joint zone (SFRC-1)
(k) Beam and slab at the mid span (SFRC-1)
(l) Beam at the mid span (SFRC-1)

Fig. 6. Comparison in the temperature-time relationships of the CFST column-RC beam frames between FEA and test results [37].

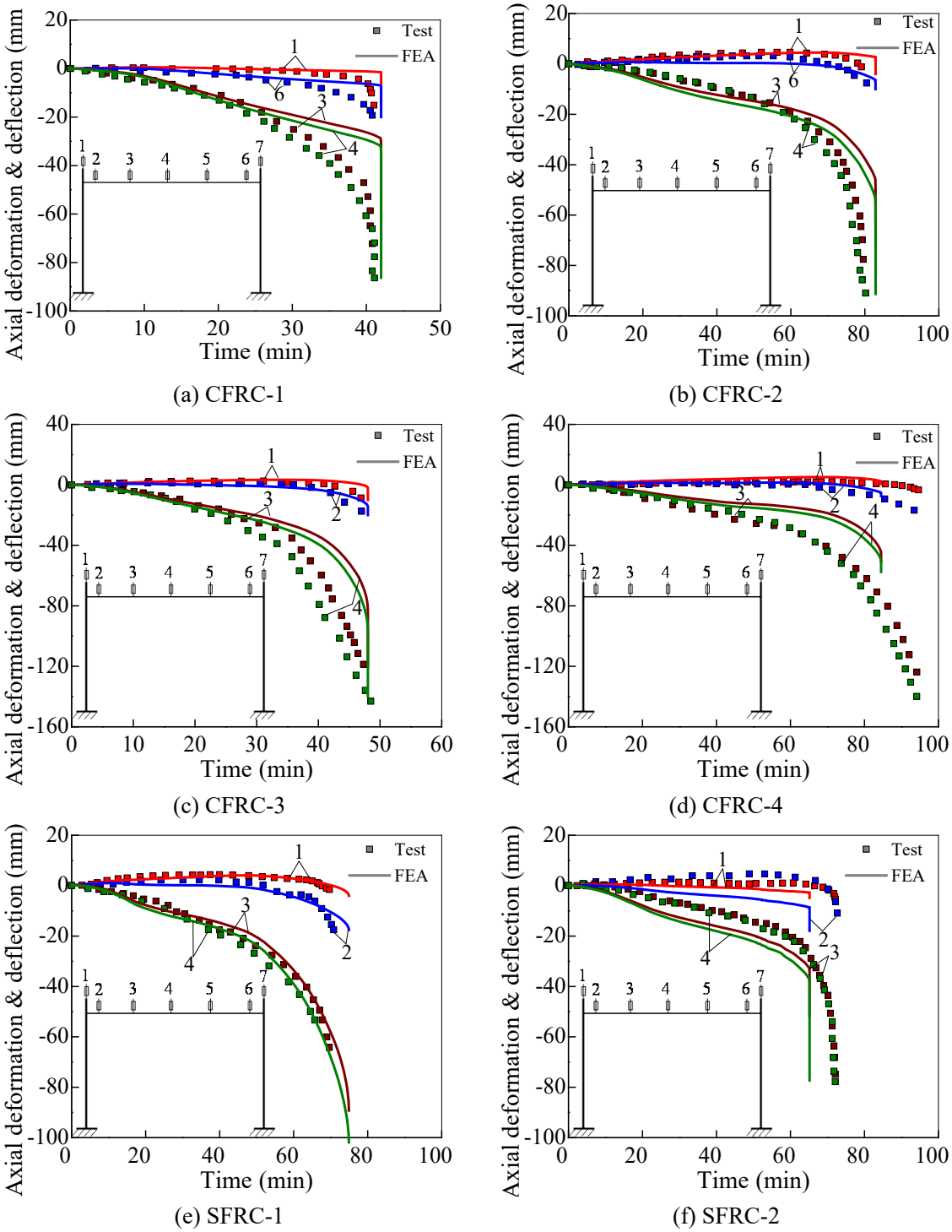

Fig. 7. Comparison in the deformation-time relationships of the CFST column-RC beam frames between FEA and test results [37].

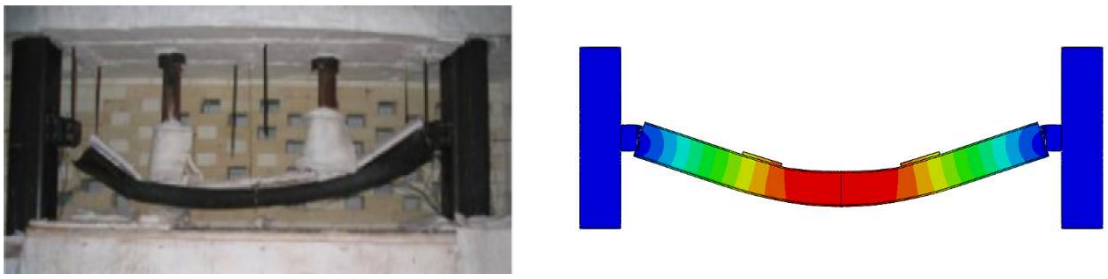

(a) Failure mode of Frame Test 4 (b) Predicted failure mode of Frame Test 4

Fig. 8. Comparison between the experimental and predicted failure modes of Ding and Wang's [39] tests.

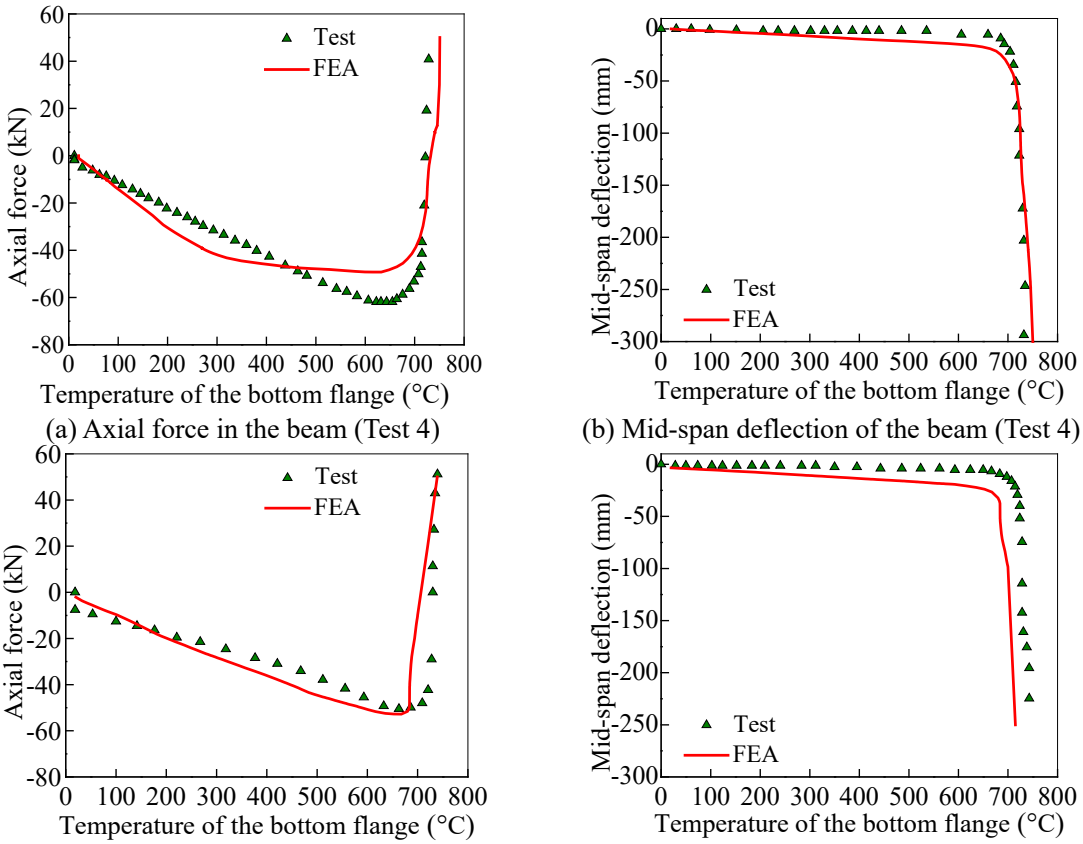

(a) Axial force in the beam (Test 4)

(b) Mid-span deflection of the beam (Test 4)

(c) Axial force in the beam (Test 8)

(d) Mid-span deflection of the beam (Test 8)

Fig. 9. Comparison in the steel beam axial force and mid-span deflection between the FEA modelling and experimental results [39].

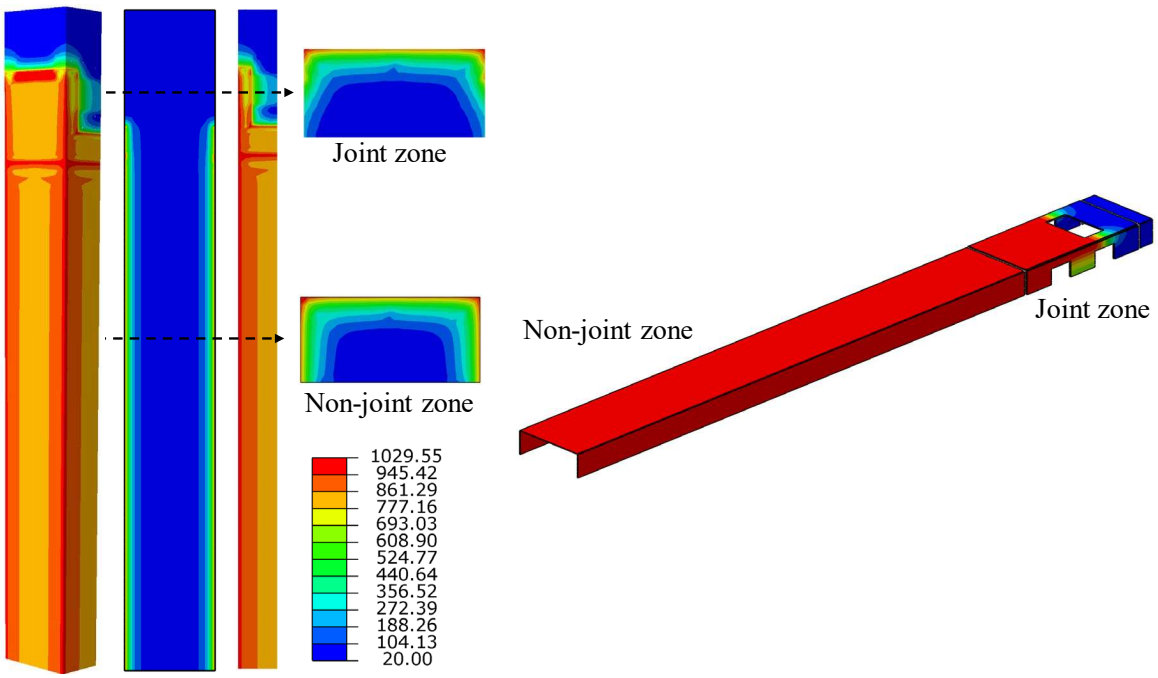

(a) Concrete and steel tube of the column

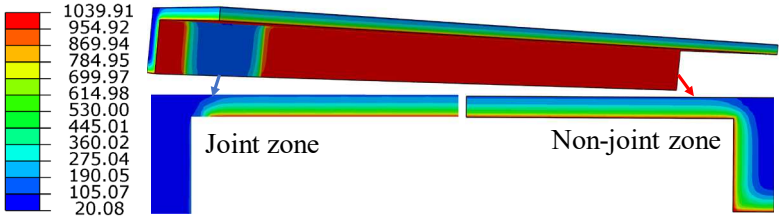

(b) Concrete of the beam and slab

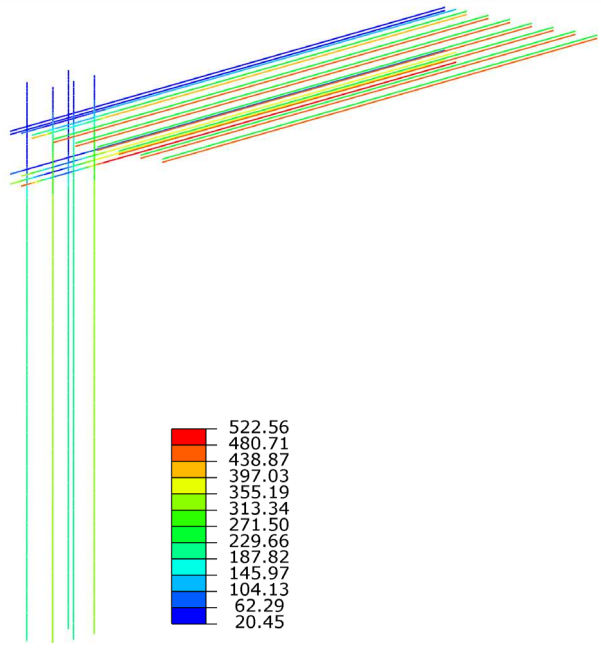

(c) Rebars in the columns, beam and slab

Fig. 10. Temperature distributions within the composite frame at 120 min (Unit: ℃).

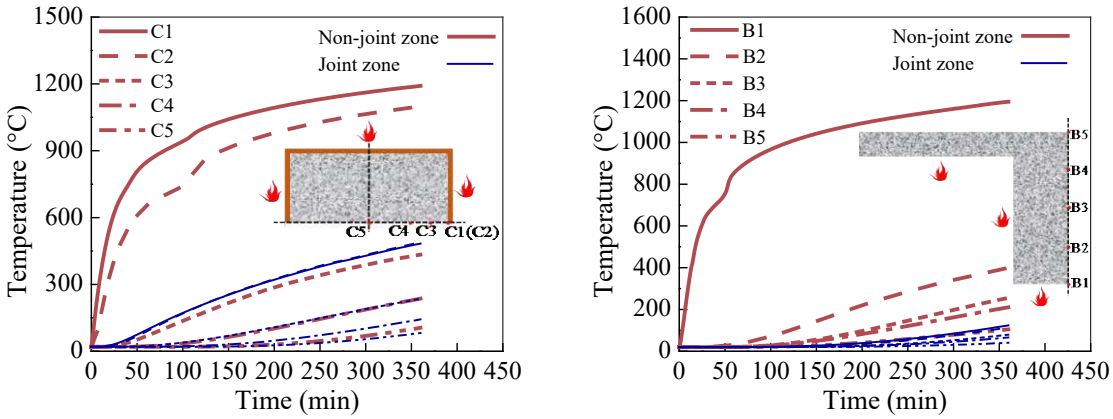

(a) Column (b) Beam

Fig. 11. The evolution of the temperature profile in the joint and non-joint zones.

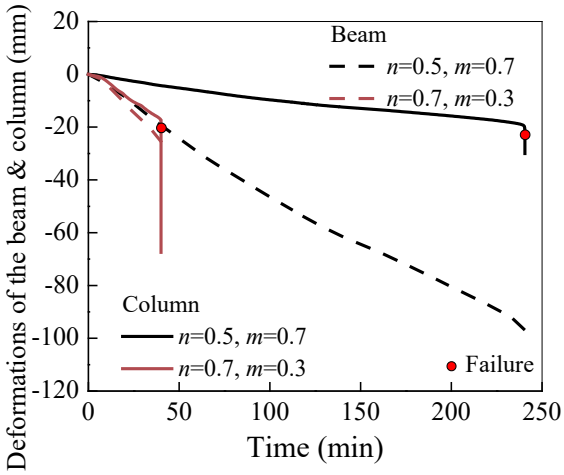

Fig. 12. The development over time of the axial deformation at column top end and that of the flexural deflection at beam mid span.

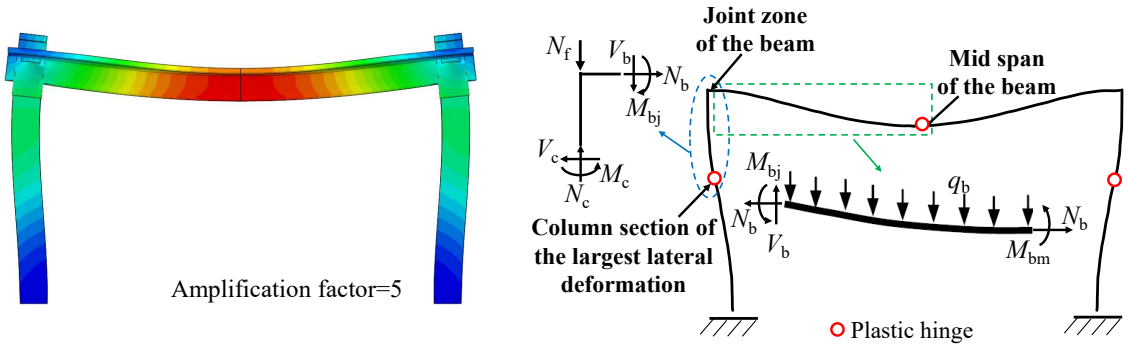

(a) Deformation shape from ABAQUS (b) Schematic of failure mechanism

Fig. 13. Deformation shape and failure mechanism of the TRC frame (n = 0.5, m = 0.5).

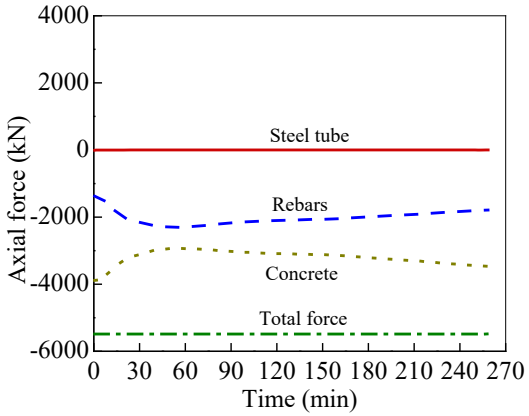

(a) Axial force in the column

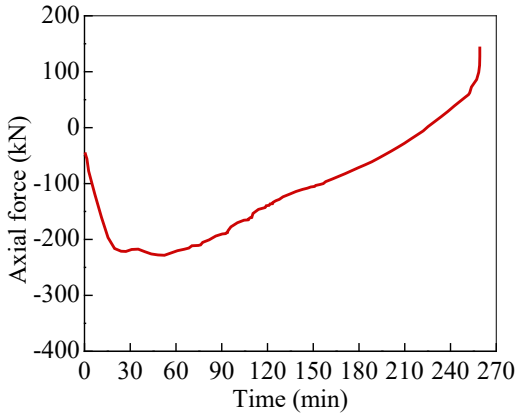

(b) Axial force in the beam

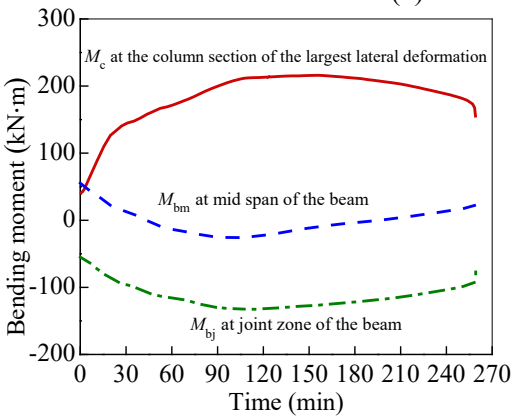

(c) Bending moments in the beam and columns

Fig. 14. Axial force and bending moment-time curves of the beam and columns (n=0.5, m=0.5).

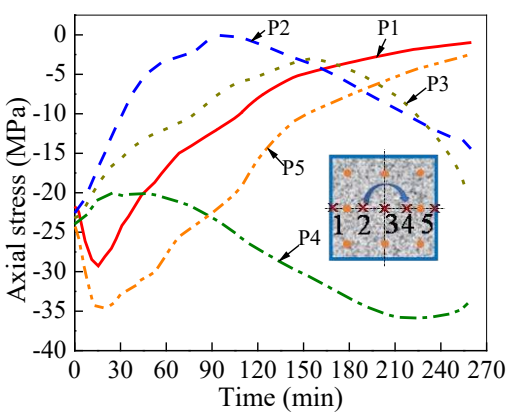

(a) Axial stresses of concrete in the column section of the largest lateral deformation

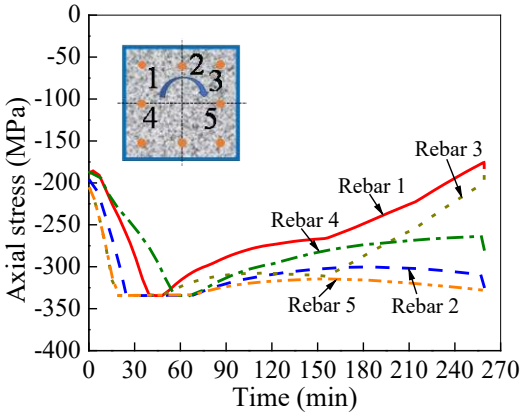

(b) Axial stresses of rebars in the column section of the largest lateral deformation

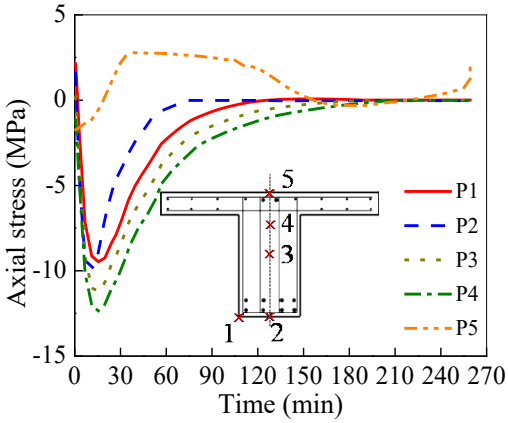

(c) Axial stresses of concrete in the mid span of the beam

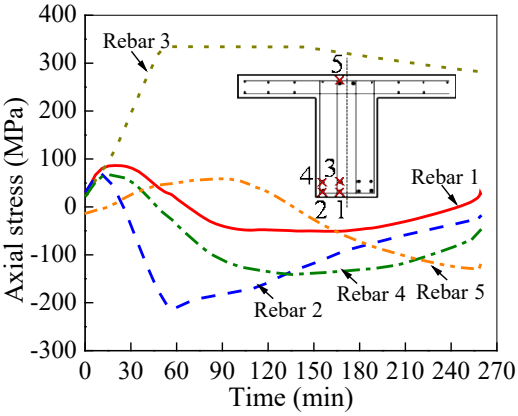

(d) Axial stresses of rebars in the mid span of the beam

Fig. 15. Axial stress vs. time relationships of concrete and rebars in the TRC columns and RC beam (n=0.5, m=0.5).

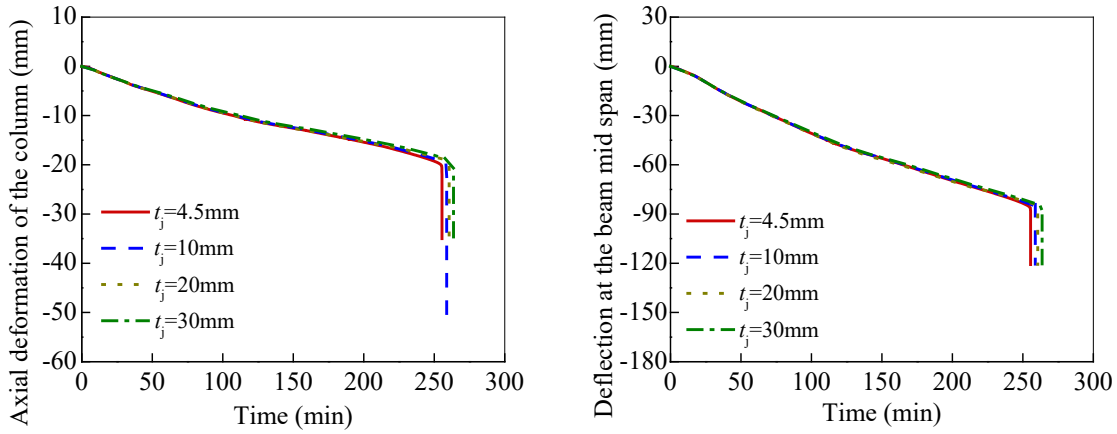

(a) Axial deformation at column top end (b) Deflection at beam mid span

Fig. 16. Influence of the thickness of the joint-zone steel tube on the high-temperature deformations of the columns and beams in the frames (n=0.5, m=0.5).

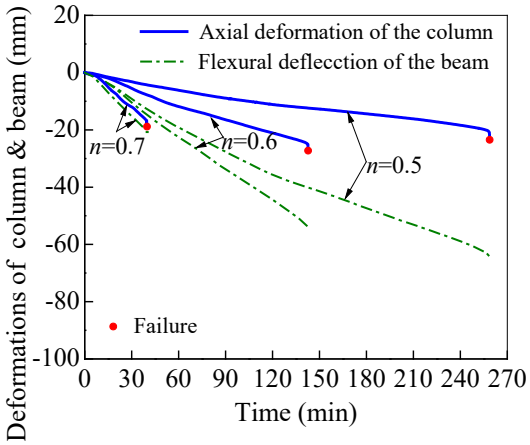

(a) Deformations of the column and beam

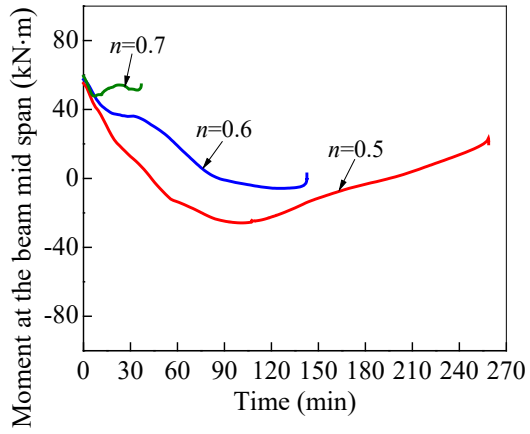

(b) Bending moment at the mid span of the beam

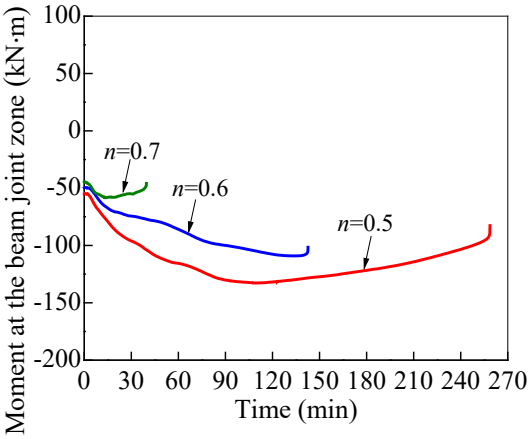

(c) Bending moment at the joint zone of the beam

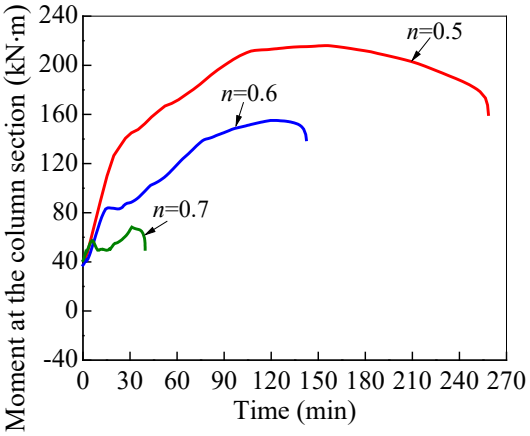

(d) Bending moment at the column section of the largest lateral deformation

Fig. 17. Influence of column load ratio on the deformations and bending moments of the TRC columns and RC beams in the frames (m=0.5).

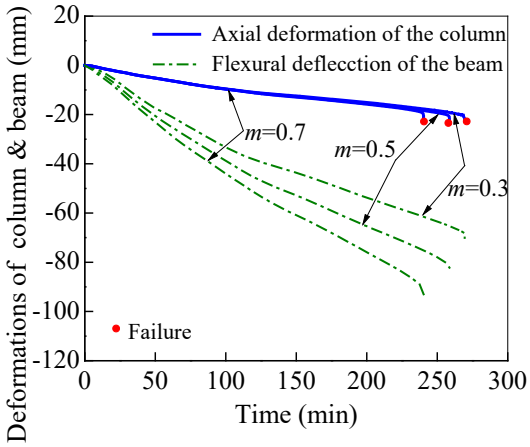

(a) Deformations of the column and beam

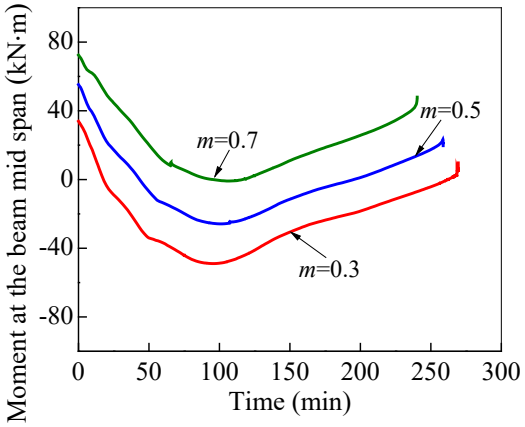

(b) Bending moment at the mid span of the beam

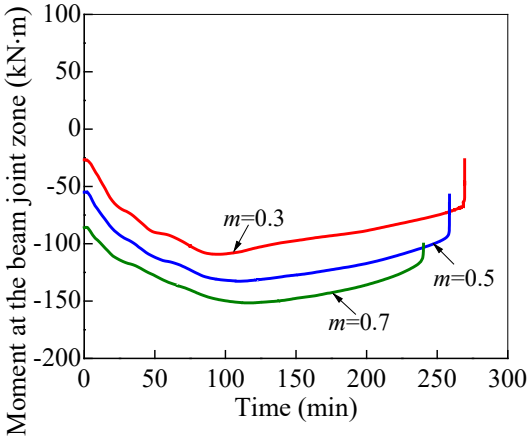

(c) Bending moment at the joint zone of the beam

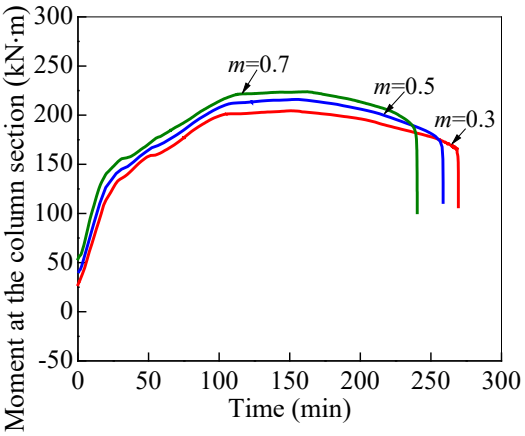

(d) Bending moment at the column section of the largest lateral deformation

Fig. 18. Influence of beam load ratio on the deformations and bending moments of the TRC columns and RC beams in the frames (n=0.5).

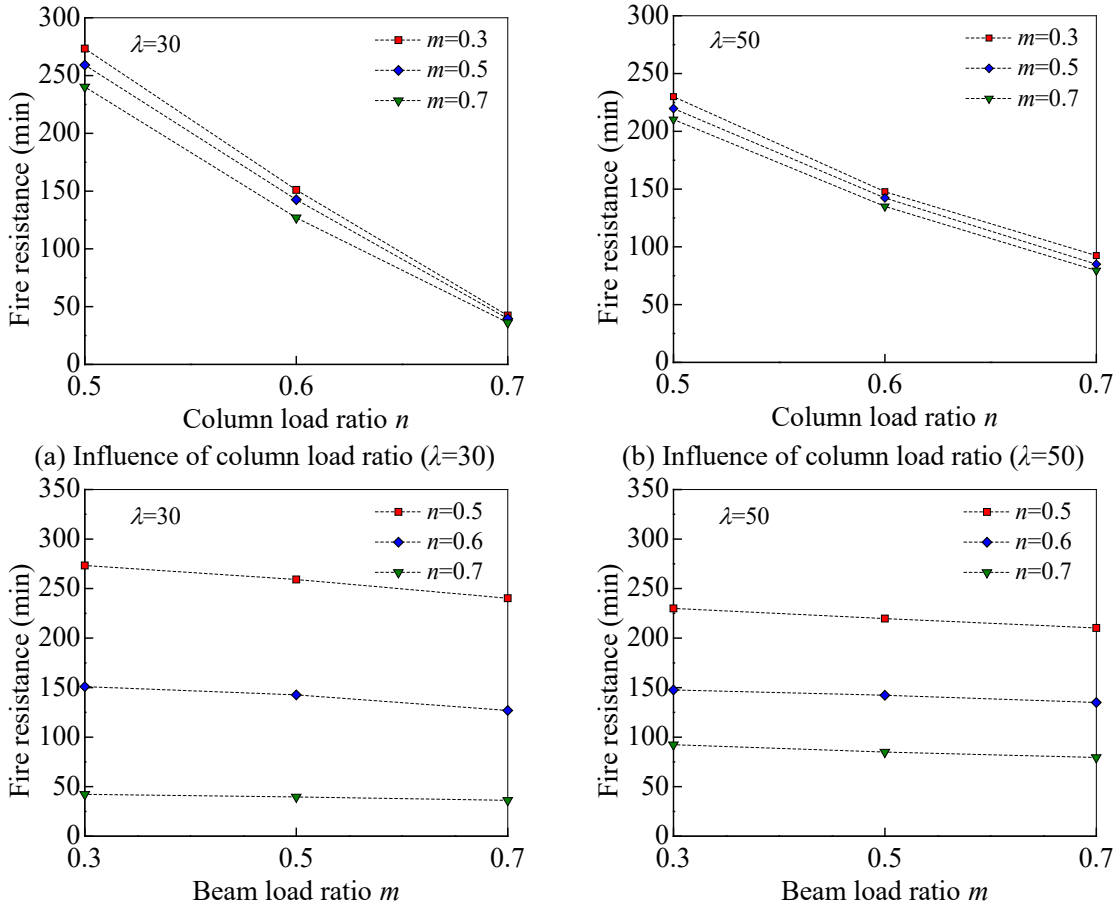

(a) Influence of column load ratio (λ=30) (b) Influence of column load ratio (λ=50)

(c) Influence of beam load ratio (λ=30) (d) Influence of beam load ratio (λ=50)

Fig. 19. Influences of column load ratio and beam load ratio on the fire resistance of the frame.

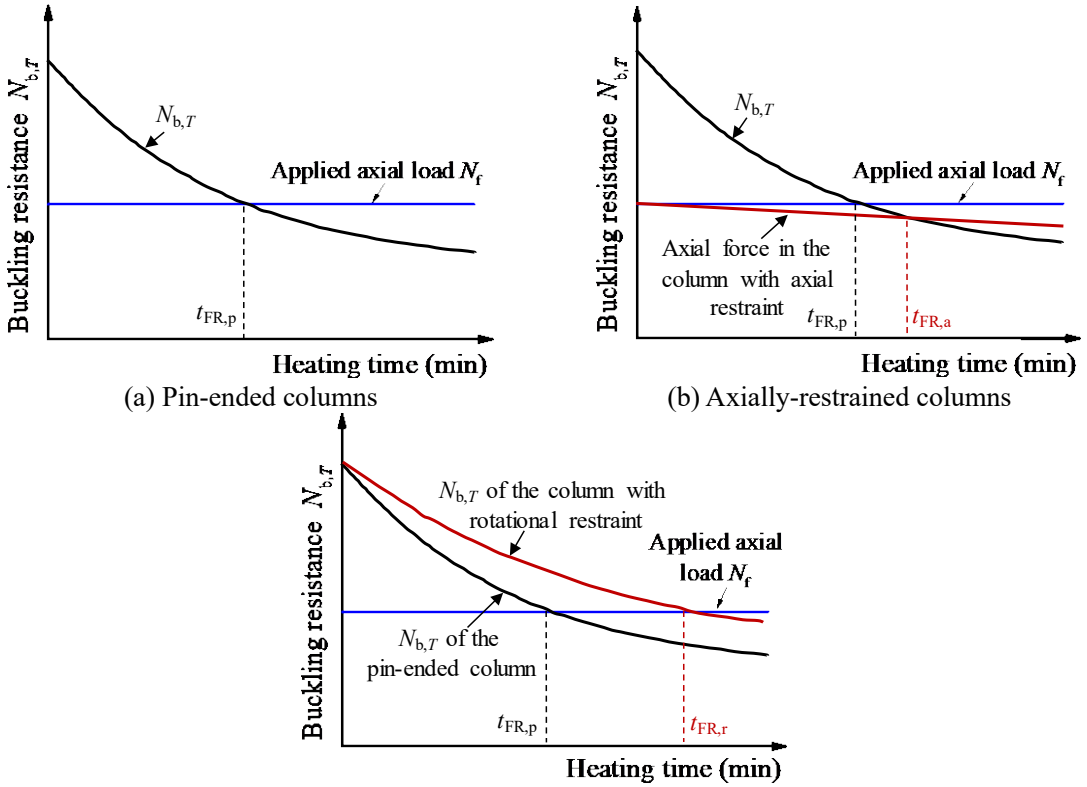

(a) Pin-ended columns (b) Axially-restrained columns

(c) Rotationally-restrained columns

Fig. 20. Effects of end restraints on enhancing the fire resistance of square TRC columns.

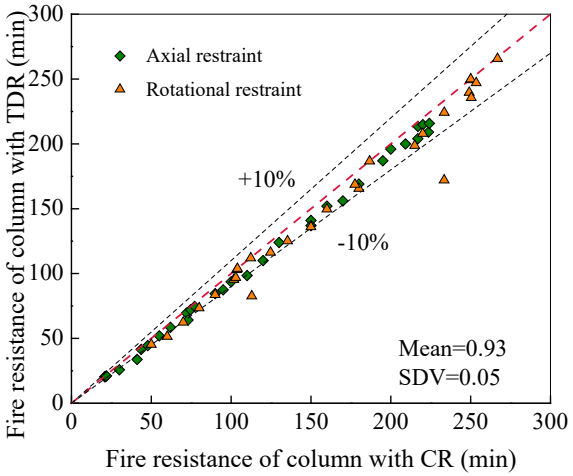

(a) Comparison of FEA simulated fire resistance between columns with TDR and CR

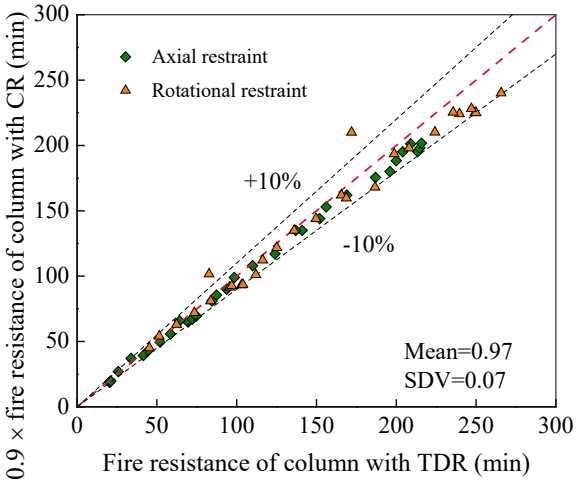

(b) Fire resistance of columns with TDR – calculated from CR columns vs. FEA

Fig. 21. Comparison of the FEA simulated fire resistance of columns with temperature-dependent and constant restraints.

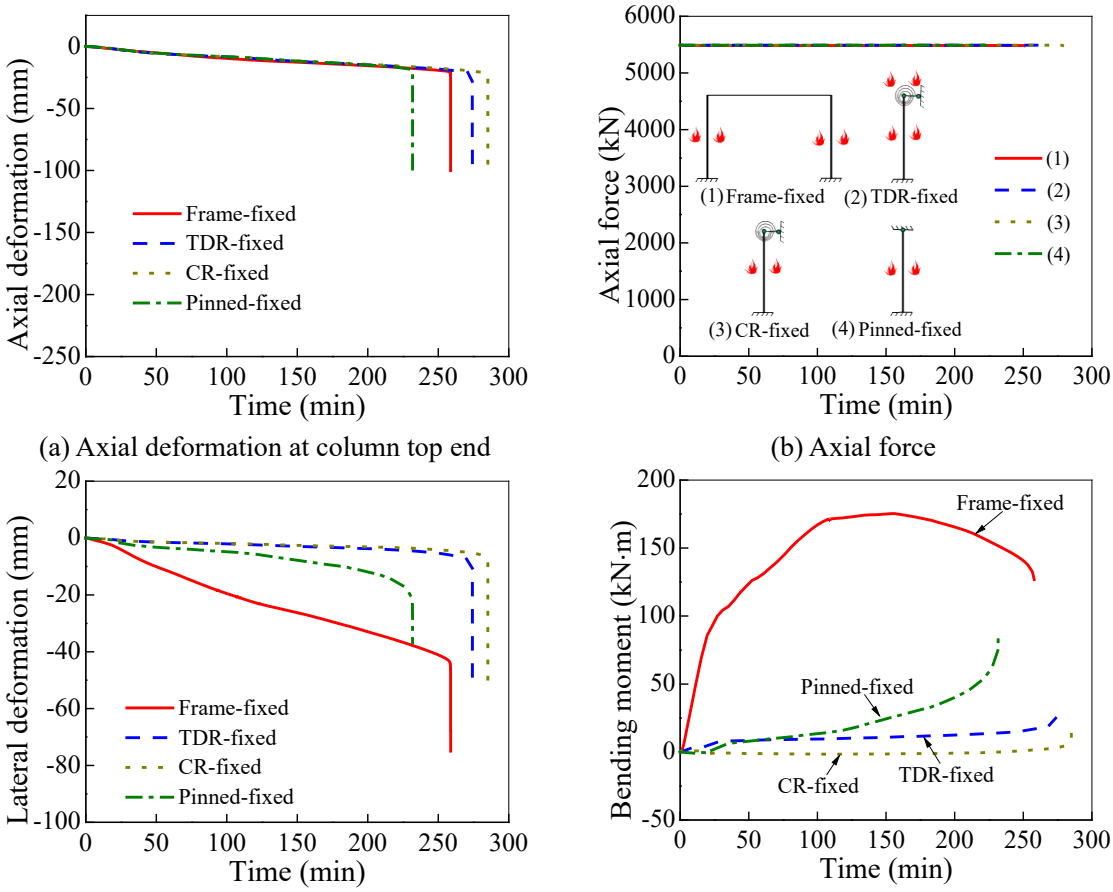

(a) Axial deformation at column top end

(b) Axial force

(c) Lateral deformation

(d) Bending moment

Fig. 22. Comparison of the axial deformation, lateral deformation, axial force and bending moment between the framed column and isolated columns (n=0.5, m=0.5).

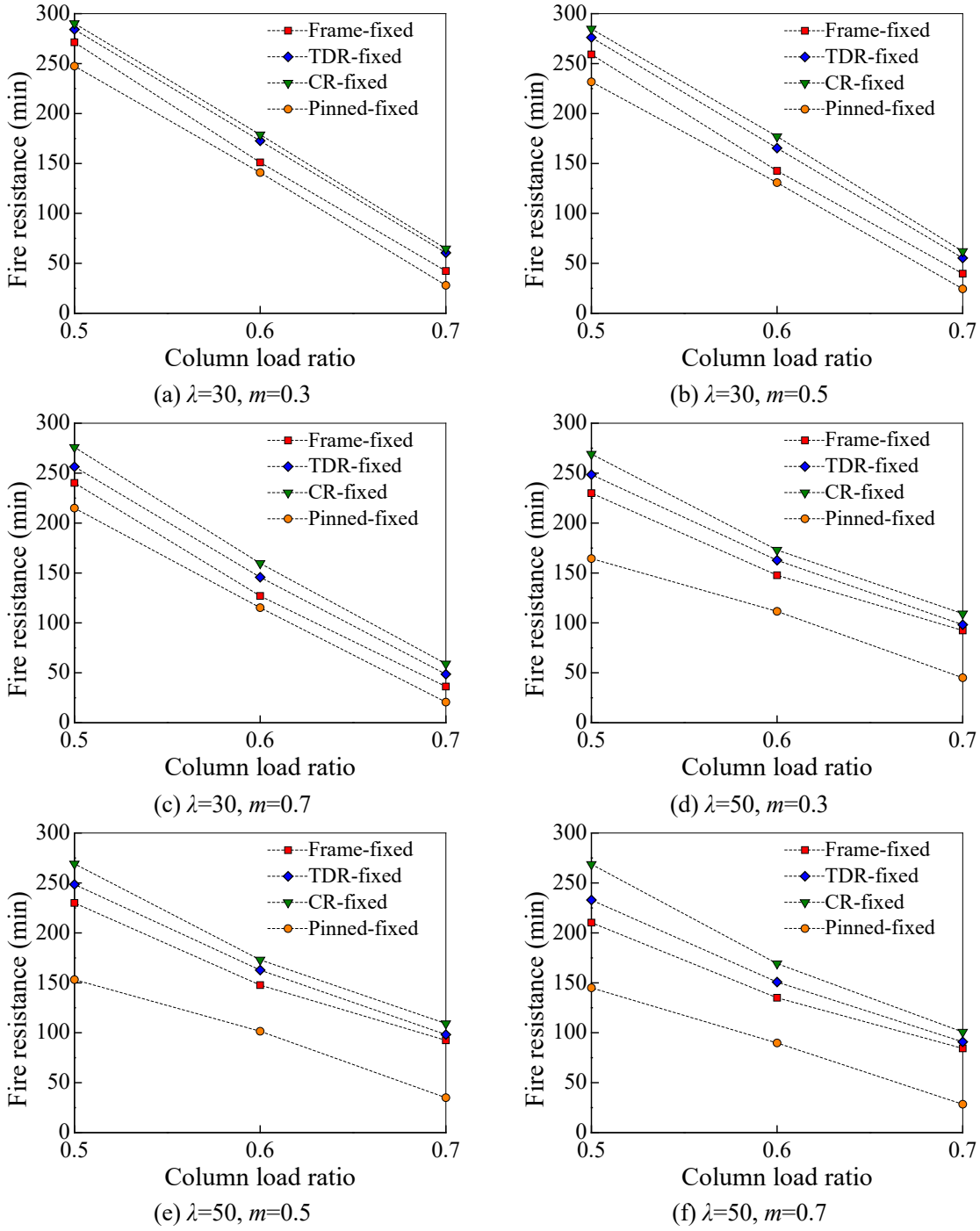

(a) λ=30, m=0.3 (b) λ=30, m=0.5

(c) λ=30, m=0.7 (d) λ=50, m=0.3

(e) λ=50, m=0.5 (f) λ=50, m=0.7

Fig. 23. Comparison of the fire resistance between the framed columns and isolated columns.

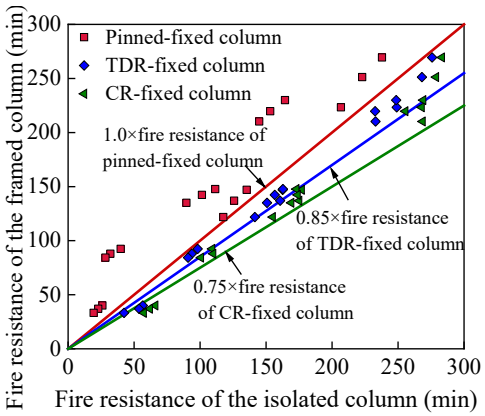

Fig. 24. A summary of the fire resistance of the framed columns and isolated columns.

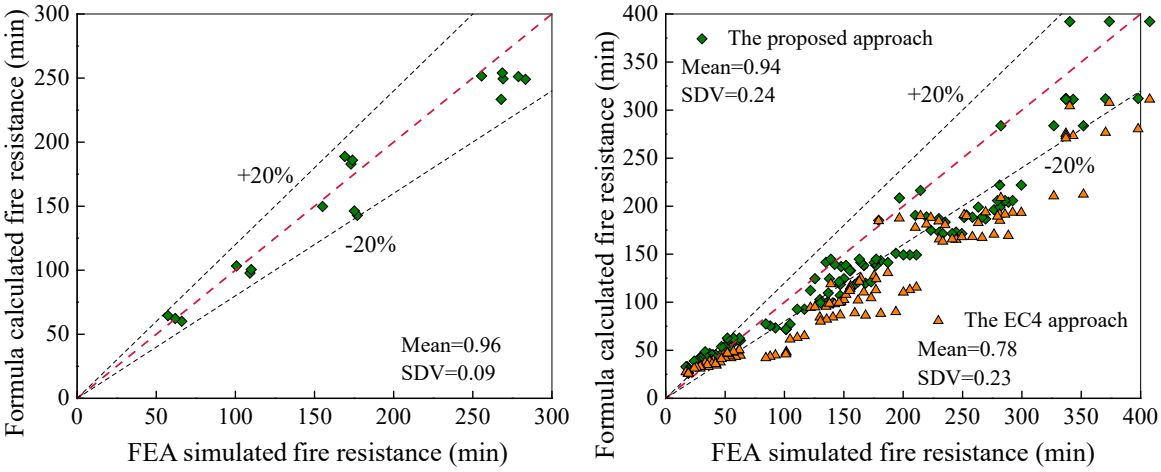

(a) Columns with constant restraints (b) Framed columns

Fig. 25. Fire resistance of TRC columns calculated with design formulae vs. FEA predictions.

Tables

Table 1

Details of the CFST column-RC beam frames tested by Han et al. [37]

Frame label	Column dimension $D\times t_s$ (mm)	Beam dimension $H_b\times B_b$ (mm)	Column load ratio n & applied load N_F (kN)	Beam load ratio m & applied load P_F (kN)	Tube yield strength f_y (MPa)	Concrete cube compressive strength f_{cu} (MPa)	Rebar yield strength f_b (MPa)	Tested fire resistance $t_{R,t}$ (min)	FEA fire resistance $t_{R,F}$ (min)	$t_{R,F}/t_{R,t}$
CFRC-1	140×3.85 (7)[a]	180×100 (2ϕ16+2ϕ12)[b]	0.58 (760)	0.3 (19.5)	412	56.7	427 (ϕ16) 445 (ϕ12)	40	43.6	1.09
CFRC-2	140×3.85 (6)[a]	180×100 (2ϕ16+2ϕ12)[b]	0.29 (380)	0.3 (19.5)	412	56.7	427 (ϕ16) 445 (ϕ12)	79	82.9	1.05
CFRC-3	140×3.85 (3)[a]	180×100 (2ϕ16+2ϕ12)[b]	0.29 (380)	0.6 (39)	412	56.7	427 (ϕ16) 445 (ϕ12)	40	48.1	1.20
CFRC-4	140×3.85 (6)[a]	160×100 (2ϕ12+2ϕ10)[b]	0.29 (380)	0.3 (11.5)	412	56.7	445 (ϕ12) 445 (ϕ10)	83	84.5	1.02
SFRC-1	140×3.51 (3)[a]	200×120 (2ϕ16+2ϕ12)[b]	0.27 (330)	0.3 (22)	263.1	56.7	427 (ϕ16) 445 (ϕ12)	70	74.9	1.07
SFRC-2	140×3.51 (6)[a]	200×120 (2ϕ16+2ϕ12)[b]	0.54 (660)	0.3 (22)	263.1	56.7	427 (ϕ16) 445 (ϕ12)	72	65.1	0.90
									Average	1.06

Notes:

[a] Thickness of the fire protection;

[b] Arrangement of reinforcing bars in the RC beam.